

Elsevier Editorial System(tm) for Progress in Oceanography  
Manuscript Draft

Manuscript Number: PROOCE-D-08-00032R2

Title: Another description of the Mediterranean outflow

Article Type: Full Length Article

Keywords: Gibraltar; Circulation; Water masses

Corresponding Author: Dr Claude MILLOT,

Corresponding Author's Institution:

First Author: Claude MILLOT

Order of Authors: Claude MILLOT

Abstract: variability of the outflow composition. Only LIW and TDW were indicated at the sill while, on the shelf, only LIW, TDW sometimes denser there than ~200 m below, and WMDW were indicated; but none of the MWs has been permanently outflowing at one or the other place. The available data can be analyzed coherently. Intermediate and deep MWs are formed in both basins in amounts that, although variable from year to year, allow their tracing up to the strait. Four major MWs circulate alongslope counterclockwise as density currents and as long as they are not trapped within a basin, which is necessarily the case for the deep MWs. In the Alboran, the intermediate MWs (WIW, LIW and upper-TDW) circulate in the north while the deep MWs (lower-TDW and WMDW) are uplifted, hence relatively motionless and mainly pushed away in the south. Since both the intermediate and deep MWs outflow at the sill, they are considered as light and dense MWs, the light-dense MWs interface possibly intersecting the AW-MWs interface in the sill surroundings. Considering an outflow east of the sill composed of only two (light-dense) homogeneous layers gives significant results. Across the whole strait, the outflow has spatial and temporal variabilities much larger than previously assumed. The MWs are superposed in the sea and lead at the sill to juxtaposed and vertically stratified suboutflows that will cascade

independently before forming superposed veins in the ocean. These veins can have similar densities and hydrographic characteristics even if associated with different MWs, which accounts for the features permanency assumed up to now. The outflow structure downstream of the sill depends on its composition upstream and, more importantly, on that of AW in the sill surroundings where fortnightly and seasonal signals are imposed on the whole outflow.

1 Another description of the Mediterranean outflow

2 Claude Millot

3 Laboratoire d'Océanographie Physique Biogéochimique

4 Antenne LOPB-COM-CNRS de La Seyne/mer, BP 330, F-83150

5 [f4eut@winlink.org](mailto:f4eut@winlink.org) and [cmillot@ifremer.fr](mailto:cmillot@ifremer.fr)

6 Abstract

7 Papers about the outflow assume that i) it is composed of only two Mediterranean Waters  
8 (MWs), the Levantine Intermediate Water (LIW) and the Western Mediterranean Deep Water  
9 (WMDW) from the eastern and western basins, respectively, ii) both MWs are mixed near 6°W,  
10 hence producing a homogeneous outflow that is then split into veins, due to its cascading along  
11 different paths and to different mixing conditions with the Atlantic Water (AW).

12 A re-analysis of 1985-1986 CTD profiles (Gibraltar Experiment) indicates two other MWs,  
13 the Winter Intermediate Water (WIW) from the western basin and the Tyrrhenian Dense Water  
14 (TDW) basically originated from the eastern basin. In the central Alboran subbasin, these four MWs  
15 are clearly differentiated, roughly lying one above the other in proportions varying from north to  
16 south. Proportions also vary with time, so that the outflow can be mostly of either eastern or western  
17 origin. While progressing westward, the MWs can still be differentiated and associated isopycnals  
18 tilt up southward as much as being, in the sill surroundings, roughly parallel to the Moroccan  
19 continental slope where the densest MWs are. The MWs at the sill are thus juxtaposed and they all  
20 mix with AW, leading to an outflow that is horizontally heterogeneous just after the sill (5°45'W)  
21 before progressively becoming vertically heterogeneous as soon as 6°15'W. There can be little LIW  
22 and/or no WMDW outflowing for a while.

1           An analysis of new 2003-2008 time series from two CTDs moored (CIESM Hydro-Changes  
2 Programme) at the sill (270 m) and on the Moroccan shelf (80 m) confirms the juxtaposition of the  
3 MWs, their individual and generally intense mixing with AW, as well as the large temporal  
4 variability of the outflow composition. Only LIW and TDW were indicated at the sill while, on the  
5 shelf, only LIW, TDW sometimes denser there than ~200 m below, and WMDW were indicated; but  
6 none of the MWs has been permanently outflowing at one or the other place.

7           The available data can be analyzed coherently. Intermediate and deep MWs are formed in  
8 both basins in amounts that, although variable from year to year, allow their tracing up to the strait.  
9 Four major MWs circulate alongslope counterclockwise as density currents and as long as they are  
10 not trapped within a basin, which is necessarily the case for the deep MWs. In the Alboran, the  
11 intermediate MWs (WIW, LIW and upper-TDW) circulate in the north while the deep MWs (lower-  
12 TDW and WMDW) are uplifted, hence relatively motionless and mainly pushed away in the south.  
13 Since both the intermediate and deep MWs outflow at the sill, they are considered as light and dense  
14 MWs, the light-dense MWs interface possibly intersecting the AW-MWs interface in the sill  
15 surroundings. Considering an outflow east of the sill composed of only two (light-dense)  
16 homogeneous layers gives significant results. Across the whole strait, the outflow has spatial and  
17 temporal variabilities much larger than previously assumed. The MWs are superposed in the sea and  
18 lead at the sill to juxtaposed and vertically stratified suboutflows that will cascade independently  
19 before forming superposed veins in the ocean. These veins can have similar densities and  
20 hydrographic characteristics even if associated with different MWs, which accounts for the features  
21 permanency assumed up to now. The outflow structure downstream of the sill depends on its  
22 composition upstream and, more importantly, on that of AW in the sill surroundings where  
23 fortnightly and seasonal signals are imposed on the whole outflow.

24           Keywords: Gibraltar, Circulation, Water masses

1	List of Contents	Page
2	1. Introduction	?
3	1.1 Current thoughts	?
4	1.2 Other thoughts	?
5	2. A re-analysis of some Gibraltar Experiment data	?
6	2.1 The 4°30'W data	?
7	2.2 The 5°00'W data	?
8	2.3 The 5°15'W data	?
9	2.4 The 5°30'W data	?
10	2.5 The 5°40'W data	?
11	2.6 The 5°50'W data	?
12	2.7 The 6°05'W data	?
13	2.8 The 6°15'W data	?
14	3. The 80-m and 270-m time series analysis	?
15	4. Discussion	?
16	4.1 Short-term variability	?
17	4.2 Seasonal variability	?
18	4.3 Long-term variability	?
19	4.4 A two-layer approximation up to the sill	?
20	4.5 A new concept of the MWs outflow	?
21	5. Conclusion	?
22	Acknowledgements	?
23	References	?
24	Figure Captions	?

## 1           1. Introduction

2           Papers about the strait of Gibraltar in general, and about the Mediterranean outflow in  
3 particular, are based on the same concept. They assume that the outflow is composed of only two out  
4 of four major Mediterranean Waters (MWs), and that both are mixed near 6°W, hence producing a  
5 homogeneous outflow that is then split into veins, due to its cascading along different paths and to  
6 different mixing conditions with the Atlantic Water (AW). This concept is supported neither by the  
7 analyses we have been conducting for a while about the functioning of the Mediterranean Sea nor by  
8 those we have recently undertaken about the Strait of Gibraltar itself. Current and personal thoughts  
9 are thus presented separately in subsection 1.1 and 1.2, respectively.

### 10           1.1 Current thoughts

11           Reliable information about the strait (Fig. 1) has been gathered from some time, and  
12 Lacombe and Richez (1982) have first specified its basic functioning, with a surface inflow of fresh  
13 Atlantic Water (salinity  $S \sim 36$ ) and a deep outflow of salty Mediterranean Water ( $S \sim 38$ ) that results  
14 from evaporation exceeding precipitation and rivers runoff in the sea. They have also emphasized  
15 the tremendous role of the internal tide in mixing the water masses and generating small-scale  
16 features.

17           Because they can easily be recognized on nearly all  $\theta$ - $S$  ( $\theta$ : potential temperature) diagrams  
18 within the western basin of the sea and within the Alboran subbasin (Fig. 2) in particular, the salty  
19 and relatively warm Levantine Intermediate Water (LIW), the intermediate water formed in the  
20 eastern basin, and the cool and relatively fresh Western Mediterranean Deep Water (WMDW), the  
21 deep water formed in the western basin, have generally been considered to be the sole components  
22 of the outflow. In a recent review paper, Baringer and Price (1999) consider the outflow to be 90%  
23 LIW and 10% WMDW, as formerly proposed by Bryden and Stommel (1984). Such proportions

1 would mean the whole sea forms mainly intermediate water, mainly in the eastern basin, and there,  
2 only in the Levantine subbasin. The constancy of these percentages, still generally accepted  
3 nowadays, suggests that no attempt has been made to improve or reconsider them.

4         Assuming an outflow composed of only LIW and WMDW, it was soon recognized (e.g.  
5 Bryden et al., 1978; Bryden and Stommel, 1982) that these MWs are found mainly in the north and  
6 south of the Alboran, respectively, while pioneering observations (Allain, 1964) mentioned the  
7 occurrence of WMDW at Camarinal Sill South (300 m; 5°45'W). The only other MW reported  
8 (Gascard and Richez, 1985) to intermittently occur in the western Alboran is the Winter Intermediate  
9 Water (WIW), the intermediate water formed in the western basin and that lies above LIW, but this  
10 observation has not been considered in subsequent papers. In addition, the possible occurrence, not  
11 only in the western Alboran but also in the western basin as a whole, of the deep waters formed in  
12 the eastern basin in both the Aegean and the Adriatic has never been mentioned, even though  
13 attention has been paid to them through the Eastern Mediterranean Transient (EMT; Roether et al.,  
14 1996).

15         After this series of general-oceanography papers, the development of two-layer hydraulic  
16 control simulations motivated new observations during the 1985-1986 Gibraltar Experiment (GE)  
17 and turned general interest towards the dynamics of flows through straits, leading to significant  
18 progress in their understanding (Bryden and Kinder, 1991). Of particular interest are the numerous  
19 and very valuable sets of cross-strait / north-south CTD transects performed using relatively high  
20 resolution sampling (2-3 nautical miles (nm) in general, sometimes less), high frequency (few days)  
21 and during several campaigns such as LYNCH-702-86, GIB1 and GIB2. We present hereafter our  
22 analysis of the GIB1 and GIB2 data mainly and show some LYNCH data west of the sill.

1 Gascard and Richez (1985) and Kinder and Parrilla (1987) inferred that LIW was found at  
2 200-600 m in the northern 2/3 of the Alboran while WMDW was found below 800 m in the central  
3 region (near 36°N) and below 400 m along the African slope. Parrilla et al. (1989) considered that  
4 LIW and WMDW have the same distribution and characteristics until almost the sill as they had in  
5 the eastern Alboran. Pettigrew (1989) definitely demonstrated the occurrence of WMDW at the sill  
6 while Kinder and Parrilla (1987) have shown its presence not only in the southern part of the sill but  
7 also few nm west of it. Then, because of active mixing processes (e.g. Wesson and Gregg, 1994),  
8 these waters were considered to become a single MW (Parrilla et al., 1989), which has been  
9 generally accepted. To our knowledge, comparative analyses of successive north-south transects of  
10  $\theta$ ,  $S$  and  $\sigma$  (the potential density anomaly), from GE and other experiments as well, have been  
11 published mainly for the Gulf of Cadiz (e.g. Ochoa and Bray, 1991; Ambar et al., 2002) and the  
12 Alboran (see above). For the strait itself, only Parrilla et al. (1989) inferred general features from  
13 transects collected during several campaigns.

14 Thereafter, and as done by Kinder and Parrilla (1987), authors no longer analyzed cross-strait  
15 transects and either inferred or performed along-strait ones. For instance, even though Bray et al.  
16 (1995) considered most of the GE data and described the 3-D characteristics of the AW-MW  
17 interface within the strait, they analyzed changes in  $\theta$ - $S$  diagrams only from west to east, not from  
18 north to south. Baringer and Price (1997, 1999) concentrated on the re-analysis of dedicated 1988  
19 data and, considering that LIW and WMDW completely mix within the strait, relied on a unique  
20 along-strait CTD transect. The homogeneous outflow assumption at the strait outlet is used in most  
21 of the recent simulations of the general circulation at ocean scale (e.g. Wu et al., 2007) and of the  
22 exchanges through the strait (e.g. Sannino et al., 2002), as well as in most of the simulations (e.g.  
23 Serra and Ambar, 2002; Johnson et al., 2002) and laboratory experiments (e.g. Davies et al., 2002)  
24 dedicated to the outflow.

1            Assuming a homogeneous outflow, it is widely accepted that basic features about its  
2 cascading from the sill are linked to its relatively high density and to the Coriolis effect while the  
3 gradual attenuation of its anomalously high thermohaline and density properties results from the  
4 mixing with the surrounding fresher and cooler AW. As a whole, the outflow then reaches quasi-  
5 equilibrium as a density current and flows northward alongslope. At 100-200 km downstream from  
6 the strait, it is said to be subdivided into two main veins at 800 and 1200 m (e.g. Siedler, 1968;  
7 Madelain, 1970) and a shallower one at 500 m (Howe et al., 1974; Zenk, 1975; Ambar, 1983) while  
8 only the two deepest veins were sometimes identified (e.g. Baringer and Price, 1997). At 6°05'W  
9 where maximum depths are 400 m, the veins were generally hard to distinguish (e.g. Baringer and  
10 Price, 1997; Ambar et al., 1999) while the two densest veins can be identified (400-700m) at 6°30'W  
11 (Borenäs et al., 2002). Following Madelain (1970), the veins have been generally attributed to the  
12 bottom topography, canyons having been expected to divert the original homogeneous outflow and  
13 cause it to mix differently with AW. Siedler (1968) hypothesized that the tidal mixing temporal  
14 variability within the strait could lead to an outflow having alternatively different characteristics,  
15 hence mainly forming two veins, while Howe et al. (1974) suggested that the upper vein originates  
16 from shallow depth in the strait.

17            According to north-south transects near 7°W (Ambar and Howe, 1979a,b), the saltiest and  
18 coolest water found in the south and the slightly fresher and warmer water found in the north should  
19 form the two deepest veins. Most recent surveys (Ambar et al., 2002) have shown that the shallowest  
20 vein has relatively high temperatures, while representative  $\sigma$  values for the cores of the three veins at  
21 their equilibrium depths are 27.4, 27.5 and 27.8 kg.m<sup>-3</sup>. In their simulations of the outflow splitting,  
22 Borenäs et al. (2002) consider that the two deepest veins at 6°30'W differ by  $\Delta\sigma \sim 0.25$  kg.m<sup>-3</sup>.

23            Additionally, Bray et al. (1995) statistically analyzed the whole GE data set. They considered  
24 a homogeneous MW and an AW composed of North Atlantic Central Water (NACW,  $\theta = 12-14$  °C,

1 S = 35.5-36.0), said to be found during all campaigns and overlaid by a modified form of NACW  
2 named Surface Atlantic Water (SAW,  $\theta = 16-22$  °C, S = 36.0-36.5). They interpreted the  $\theta$  and S  
3 distributions within the strait as a mixture of these three principal water types and inferred typical  
4 percentages for an upper, an interface and a lower layer, as well as seasonal and east-west variations.

## 5 1.2 Other thoughts

6 We already mentioned (Milot, 1999; Milot and Taupier-Letage, 2005a) that significant  
7 WIW amounts occurred in the Alboran and commented on the importance of the Tyrrhenian Dense  
8 Water (TDW) that results from the deep eastern waters cascading into the western basin. The  
9 hydrographic characteristics in the sea of AW and the four major MWs are synthesized in 1.2.1.

10 We also described in these papers the AW and MWs circulation in the whole sea and  
11 explained why, according to the Coriolis effect, they circulate alongslope counterclockwise as  
12 density currents looking like veins, except when they are trapped, as is necessarily the case for the  
13 densest part of WMDW in the deepest part of the western basin. A new schematization of the  
14 circulation in the western basin is proposed in 1.2.2.

15 Additionally, we specified some aspects of the outflow variability in both the long term  
16 (decades; Milot et al., 2006) and the short term (weeks; Milot, 2008). In this last paper we have  
17 also shown that the outflow characteristics in the Atlantic depend more on the nature of AW in the  
18 sill surroundings than on the outflow composition east of the sill. At medium scales (seasons-years),  
19 the role of the MWs-AW mixing in defining the outflow characteristics is made more complex by  
20 the large seasonal variability and huge interannual increase of the AW salinity (Milot, 2007). Our  
21 own results at Gibraltar are summarized in 1.2.3.

### 22 1.2.1 The waters hydrographic characteristics

1           Due to intense mixing in the sill surroundings, the  $\theta$  and S extrema that characterize the  
2 various MWs markedly reduce from east to west of the sill so that the numerical values given  
3 hereafter are the extrema expected in the western Alboran. Some MWs are structured like veins and  
4 these extrema are those associated with their cores. Therefore, they cannot be specified accurately  
5 either with hydrographic sections, even when performed with a sampling interval as small as 2-3 m,  
6 or with time series at fixed locations. They could be accurately specified only with tow-yow devices,  
7 which cannot be envisaged in the long-term. Other MWs approaching the sill are already mixed with  
8 AW so that actual extrema are markedly depth dependent. Note that, even though the  $S_{\min}$  associated  
9 with NACW can be recognized in most of the sea, it markedly reduces from west to east.

10           WIW results from AW cooling in the Provençal and the Ligurian (Fig. 2) and can represent  
11 relatively large amounts of transformed AW. It was recognized in the strait (Gascard and Richez,  
12 1985) and it is said to occur intermittently in the Alboran (Vargas-Yanez et al., 2002), being  
13 characterized by  $\theta_{\min}=12.9-13.0$  °C at 100-300 m. Even though never described in the GE papers, it  
14 is clearly indicated on most GE CTD transects east of the sill (see section 2).

15           LIW is the most known of all MWs, partly because it is clearly indicated on  $\theta$  and S profiles  
16 in most of the sea by relative and absolute maxima, respectively, hence forming a bump on a  $\theta$ -S  
17 diagram. However, it is generally forgotten that, along its route from the Levantine to Gibraltar, LIW  
18 is involved in the formation of dense MWs in the Aegean, the Adriatic and the Provençal. Therefore,  
19 in addition to its own variability in both amount and characteristics when formed, and to its more or  
20 less continuous mixing with surrounding MWs all along its route, a specific variability is imposed by  
21 these wintertime events. In the end, the variability is so complex that any type of seasonality can  
22 hardly be observed at Gibraltar. In the Alboran,  $\theta_{\max}=13.1-13.2$  °C (200-400 m) and  $S_{\max}=38.50-$   
23  $38.52$  (300-500 m). Since the waters above (WIW) and below (TDW) LIW have rarely, if not never,

1 been considered, and as mixing prevents to any separation between them, all these MWs were  
2 considered as being LIW, which led assuming that LIW represents up to 90% of the outflow.

3 TDW results from the mixing of the eastern basin deep MWs (EMDW, by analogy with  
4 WMDW) with the MWs resident in the Tyrrhenian. In the Channel of Sicily (sills at 400 m, north-  
5 south oriented), EMDW is differentiated from LIW mainly by lower  $\theta$  (14.0 vs. 14.5 °C), the  
6 EMDW (respectively LIW) core being along the Tunisian/western (respectively Sicilian/eastern)  
7 slope. Unmixed EMDW is denser than WMDW (29.15 vs. 29.10 kg.m<sup>-3</sup>). When Sparnocchia et al.  
8 (1999) reported the cascading of the eastern basin outflow down to ~2000 m, we commented on the  
9 regulation of the WMDW amount such a cascading (of only EMDW) would lead to. If the WMDW  
10 amount is relatively low, only the WMDW uppermost part will mix with EMDW and TDW will be  
11 mainly of eastern origin, its upper part circulating like LIW. If the WMDW amount is relatively  
12 large, more of it will mix with EMDW and TDW will be more of western origin, its lower part  
13 behaving like WMDW. Obviously, such a WMDW regulation and the TDW characteristics also  
14 depend on the EMDW amount and on the fact that not only WMDW but also old LIW and old TDW  
15 (see 1.2.2) can be found at 400-2000 m in the Tyrrhenian. The relatively large  $\sigma$  of the MWs  
16 resident there, compared to that of the cascading EMDW, leads to a TDW outflow much thicker than  
17 the outflow from Gibraltar that is about twice as large. TDW lies in between the well-known LIW  
18 and WMDW and more or less mixes with them, while, on a  $\theta$ -S diagram, it is located not far from a  
19 LIW-WMDW mixing line, which partly explains why it is currently ignored. TDW does not have a  
20 well-defined core in the ranges  $\theta=13.0$ -13.1 °C and S=38.48-38.51. We differentiate hereafter, for  
21 convenience, a lower-TDW from an upper-TDW that will behave more like WMDW and LIW,  
22 respectively, but TDW has nothing to do with LIW.

1           The fact that the cool (12.9-13.0 °C) and relatively fresh (38.44-38.48) WMDW, formed by  
2 deep convection mainly in the Provençal (~2000 m), can be the densest of the MWs in the western  
3 basin has consequences for the outflow that have not been emphasized enough. Indeed (see details in  
4 1.2.2), first note that WMDW formed during a specific winter can be more or less dense. The  
5 densest WMDW cascades over the bottom at depths >2000 m only, circulates counterclockwise  
6 along the continental slope, and is first trapped in the Algerian and the Tyrrhenian before being  
7 uplifted more and more by newly formed denser WMDW. The less dense WMDW never reaches  
8 depths of 2000 m, mixing and spreading there without circulating significantly. In most of the  
9 Alboran (<1500 m), the WMDW specificity is thus that it does not circulate significantly and is  
10 markedly mixed, although possibly relatively young or very old. The linear trends (+0.03 °C/decade  
11 and +0.01/decade over four decades) in the deeper part of the Provençal (Béthoux et al., 1990)  
12 cannot be specified in the study area (Millot et al., 2006).

### 13           1.2.2 The circulation of the waters

14           Figure 2 schematizes, for the western basin and in only one diagram, the set of three  
15 diagrams we previously proposed for the circulation of AW and the major MWs in the whole sea.  
16 Basically, AW and the MWs circulate as density currents according to processes that are exactly  
17 those currently admitted for the cascading and circulation of the Mediterranean outflow northward,  
18 due to rotation. Within such a relatively closed basin, all waters thus circulate initially as veins  
19 (continuous lines in Fig. 2), alongslope and counterclockwise. Peculiarities about the driving forces  
20 and equilibrium levels are: i) AW flows into the sea to compensate for its water deficit, hence for the  
21 sea level difference between the sea and the ocean, ii) WIW and WMDW formed in the north of the  
22 basin are first amassed locally in late winter, above LIW for WIW or on the bottom for WMDW,  
23 before spreading all year long, iii) LIW continues its route from the Levantine without being  
24 disturbed by its passage through the Channel of Sicily, iv) EMDW cascades from this channel and

1 leads to TDW. Note that only the upper-TDW is identified in Fig. 2 while the lower-TDW is not  
2 differentiated from the relatively motionless WMDW upper part (see below). Within most of the  
3 basin, we thus consider a set of intermediate MWs (WIW+LIW+upper-TDW) and a set of deep ones  
4 (lower-TDW+WMDW). Also note i) the non-occurrence along the African slope of any intermediate  
5 vein, ii) that intermediate MWs entrained in the Algerian interior mix there until no longer  
6 associated with any horizontal density gradient, hence no longer circulating and forming old LIW  
7 and old TDW somehow trapped in the basin and possibly entering the Tyrrhenian to be involved in  
8 the formation of new TDW.

9           When newly formed WMDW is dense enough to reach the bottom in the Provençal (~2000  
10 m), it amasses there before spreading and circulating at greater depths that correspond to its  
11 equilibrium level. Such a WMDW surrounds the Balearic Islands (the channel is 800 m deep) and  
12 skips most of the Alboran (depths <1500 m). Since the Channel of Sardinia is only 2000 m deep,  
13 WMDW circles in the Algerian (2900 m) where huge yearly means of  $\sim 10 \text{ cm.s}^{-1}$  were measured at  
14  $\sim 2700$  m off Algeria (Millot and Taupier-Letage, 2005b). This young WMDW is thus trapped there  
15 and it uplifts the older but still relatively dense WMDW. Only the part of this older WMDW lifted  
16 above 2000 m can outflow into the Tyrrhenian (3500 m), where it will circulate, mix and be trapped  
17 as long as not uplifted by denser WMDW. In the Provençal, when newly formed WMDW is not  
18 dense enough to reach the bottom, it sinks in a continuously stratified layer of old WMDW and  
19 mixes locally at depths <2000 m, hence not circulating.

20           WMDW (and lower-TDW) found at depths much shallower than 2000 m (i.e. <1500 m) thus  
21 does not circulate significantly, be it newly formed in the Provençal, uplifted in the Algerian and the  
22 Tyrrhenian, or markedly mixed anywhere. Due to the Coriolis effect, both the intermediate MWs  
23 and AW that circulate alongslope depress the motionless deep MWs by several 100s m in both the  
24 north and the south of the Alboran so that, when intermediate MWs do not spread far to the south,

1 the deep MWs can reach shallow levels in between. Since WMDW is formed nearly every winter, it  
2 has to outflow from the sea so that it must proceed towards the strait and up to its sill depth. One  
3 reason leading to such a westward and upward motion that has never been envisaged up to now  
4 could be the WMDW permanent occurrence up to very shallow depths (<100 m) in the Provençal,  
5 which could lead to WMDW pressed upward everywhere else. Whatever the case, in the Alboran, i)  
6 WMDW cannot be structured as a vein, so that its average westward speed is necessary low, ii) its  
7 age and characteristics cannot be specified, iii) it is more or less mixed, iv) it is mainly located in the  
8 south where the intermediate MWs hardly spread.

9         Considering that both the "intermediate" and the "deep" sets of MWs outflow at depths <300  
10 m, we have found it more correct to deal thereafter with sets of "light" vs. "dense" MWs.

### 11         1.2.3 Recent results at Gibraltar

12         The CIESM Hydro-Changes Programme ([ciesm.org/marine/programs/hydrochanges.htm](http://ciesm.org/marine/programs/hydrochanges.htm),  
13 HCP) initiated in the early 2000s maintains moored CTDs (Sea-Bird SBE37-SMs) in the whole sea.  
14 The CTD sensors are flushed before sampling, mainly to prevent sedimentation on the conductivity  
15 cell. Adequate nominal accuracies (0.002 °C, 0.0003 S/m), resolution (0.0001 °C, 0.00001 S/m) and  
16 stability (0.0024 °C/yr, 0.0036 S/m/yr), as well as a multi-year autonomy (1-h sampling), yield  
17 deployment duration limited mainly by the mooring resistance. Among others, two CTDs are  
18 operated since January 2003 in the strait (Fig. 1), one at Camarinal Sill South (270 m) the other on  
19 the Moroccan shelf (80 m). They were serviced in April 2004, November 2005, March 2007 and  
20 October 2008. Calibrations made by the manufacturer before January 2003 and after November 2005  
21 and March 2007 give drifts (in °C/yr and S/m/yr) at both 80 m and 270 m much lower than the  
22 nominal values. Assuming linear drifts during these 33-month and 16-month periods allowed us to  
23 check the time series continuity. The CTDs used from March 2007 to October 2008 are not post-

1 calibrated yet, so that data are not shown hereafter and just commented. Resulting from the short  
2 mooring length (10 m) and the GPS accuracy, positions / immersions are easily maintained (as  
3 confirmed at the recovery). The data set is thus very reliable.

4         The 2003-2004 time series from the 270-m CTD and other ones from previous experiments  
5 indicate (Millot et al., 2006) that the outflowing MWs have been temporarily warming and becoming  
6 more saline since the mid 1990s, being in the early 2000s much warmer ( $\sim 0.3$  °C) and saltier ( $\sim 0.06$ )  
7 than  $\sim 20$  years ago. Only LIW and upper-TDW, i.e. light MWs, were found at the sill without any  
8 dense MWs. As a probable consequence of the EMT, TDW was more of eastern origin than  
9 previously; but even more eastern TDW has been encountered since then (see below). The 80-m  
10 CTD, set to monitor the inflow, in fact allows monitoring both the inflow and part of the outflow,  
11 due to the large amplitude of the internal tide (Millot, 2007). The inflow shows a marked seasonal  
12 variability of S (amplitude  $\sim 0.5$ , maximum in winter), due to air-sea interactions, and a huge  $\sim 0.05$   
13  $\text{yr}^{-1}$  interannual salinification during the 2003-2007 period. Examples of the time series recorded at  
14 both places are given in both papers and a schematic diagram of the MWs distribution at the sill is  
15 proposed in Millot et al. (2006).

16         We already looked for comparisons with more standard hydrographic data and considered the  
17 very valuable GE transects. Even though the LYNCH campaign only focused on the strait itself, it is  
18 interesting since transects were repeated several times within two weeks from  $5^{\circ}15'W$  to  $6^{\circ}05'W$  that  
19 were assumed to be the strait entrance and outlet for the MWs. In addition, marked changes occurred  
20 during the campaign in the composition of both the set of MWs east of the sill and AW (NACW vs.  
21 SAW). Due to mixing, the outflow overall characteristics west of the sill depend less on the  
22 composition of the set of MWs than on that of AW (Millot, 2008).

1           The marked differences between the current thoughts and our personal ones led us to  
2 reconsider the former, and we deal hereafter with a "MWs outflow" (not MW outflow) to emphasize  
3 its expected heterogeneity. We describe the outflow characteristics first with a re-analysis of GE  
4 CTD profiles (mainly GIB1 and GIB2, section 2) and then with an analysis of the full HCP CTD  
5 time series (section 3). We discuss both analyses in section 4 before concluding in section 5.

## 6

### 7           2. A re-analysis of Gibraltar Experiment data

8           A series of north-south CTD transects across the Alboran subbasin, the Strait of Gibraltar and  
9 the Gulf of Cadiz were repeated several times during several GE campaigns in 1985-1986 (Fig. 1).  
10 The LYNCH-702-86 (November 1985), GIB1 (March-April 1986) and GIB2 (September-October  
11 1986) data available in the MEDATLAS database (MEDAR group, 2002) are of particular interest  
12 and we analyzed all the profiles available between  $4^{\circ}30'W$  and  $6^{\circ}15'W$ . The interest of the LYNCH  
13 data was already specified (in 1.2.3) and some data are shown hereafter. The GIB1 and GIB2 data  
14 are interesting because, even though transects were not repeated, they covered the whole study area  
15 within one week. The features indicated in the GIB1 and GIB2 transects suggest relatively stable  
16 dynamical regimes during both campaigns, making them suitable for a description of the outflow,  
17 and significant differences between them illustrate some aspects of the variability. We thus present  
18 hereafter mainly the GIB1 and GIB2 data (Fig. 1, Tab.1). More accurate locations can be found in  
19 the literature. Dates and times in Tab.1 define the profiles we considered.

20           The GIB1 and GIB2 transects are all of great value since they were performed with relatively  
21 small sampling intervals, ranging from  $\sim 2$  nm (sometimes less) in the strait to  $\sim 3$  nm outside of it,  
22 generally down to a few metres above the bottom, and as rapidly as possible. The longest deepest  
23 transects ( $4^{\circ}30'W$ ,  $5^{\circ}00'W$ ,  $5^{\circ}15'W$ ) were completed in 10-15 h and the shortest shallowest ones

1 (5°30'W, 5°40'W, 5°50'W, 6°05'W, 6°15'W) in 4-6 h. These eight transects were not always  
2 performed successively, which led to overall surveys lasting about a week while the required  
3 minimum is about four days. As done by all previous authors, we consider that these transects are  
4 representative of a synoptic situation and do not depend on the relatively important tidal mixing  
5 variability with time. As usually, we thus consider only the mixing variability with space.

6         When analyzing hydrographic transects so different in both north-south extent (4 to 70 nm)  
7 and maximum depth (300 to 1400 m) with figures drawn with different y-z scales and focusing on  
8 the locations where data are available, one must keep in mind the areas these transects actually  
9 represent as well as the consequences for both the MWs outflow and the AW inflow. For instance  
10 (Fig. 3), the transports of both the outflow and the inflow through the 4°30'W section (90 nm, 1400  
11 m) being similar to those through the sill/5°45'W section (20 nm, 300 m), which has an area about  
12 30 times less, the distribution and speed of both flows markedly vary from one section to the other.  
13 Figure 3 also allows an overview of the GIB1 and GIB2 data. East of the sill, the  $\sigma = 28.75 \text{ kg.m}^{-3}$   
14 isoline is assumed to represent the AW-MWs interface while, as argued later on, separation of the  
15 light and dense MWs can be done with  $\sigma = 29.08 \text{ kg.m}^{-3}$ ; west of the sill, other representative values  
16 were chosen. Figure 3 helps understand the difficulty of the sampling since ship drifts during a CTD  
17 profile can be relatively important due to large currents, not considering navigational constraints and  
18 commercial traffic. Even though the bathymetry can be relatively steep, the fact that most of the  
19 profiles were made down to a few metres above the bottom helps ensure that, in general, no  
20 significant amount of the MWs was missed. Figures are drawn using all data available in the  
21 MEDATLAS database with pressure intervals of 2 dbar for GIB and 1 dbar for LYNCH.

22         Data are analyzed from west to east and for GIB1 and GIB2 simultaneously, first with  $\theta$ -S  
23 diagrams, then with y-z sections for  $\theta$ , S and  $\sigma$ . The  $\theta$ -S diagrams for all sections between 4°30'W

1 and 5°50'W are drawn with the same scales and with acronyms specified at exactly the same  
2 positions to facilitate profiles comparisons. Those from 5°50'W to 6°15'W are drawn with extended  
3 scales to represent more data. Profiles that clearly indicate in their upper part the WIW and/or LIW  
4 cores, hence light MWs, are plotted in red. Those indicating dense MWs only are plotted in blue  
5 while the ones indicative of both light and dense MWs are plotted in violet. As expected (subsection  
6 1.2), a general result will be that red profiles are in the north, blue profiles in the south and violet  
7 profiles in between. To simplify the analyses, the correspondence between the shape of the profiles  
8 (i.e. the MWs they evidence) and their location (in a north-south direction) is not emphasized. Also,  
9 the measured extrema, in particular those associated with the light MWs, do not regularly reduce  
10 westward up to the sill, which is due to a still too large sampling interval for MWs structured as  
11 veins, not considering their own heterogeneity.

## 12 2.1 The 4°30'W data

13 The  $\theta$ -S diagrams in Fig. 4 indicate all four major MWs during both GIB1 and GIB2. WIW  
14 was more clearly noticed during GIB2 (12.9-13.0 °C, 38.25-38.35) than during GIB1 (~13.05 °C,  
15 ~38.25) while LIW was less mixed during GIB1 (13.05-13.10 °C, 38.45-38.47) than during GIB2  
16 (~13.05 °C, ~38.45). Several GIB1 and two GIB2 red profiles indicate low WIW amount, hence a  
17 direct AW-LIW mixing. The deepest among the red profiles also indicate, below LIW, both TDW  
18 and WMDW. Note that TDW is indicated by the curved shape of the diagrams between LIW and  
19 WMDW, which cannot result from a mixing between only LIW and WMDW.

20 During GIB1 (Fig. 4a), two violet profiles only indicate lower-TDW (not WMDW) in their  
21 deeper part, then heterogeneities clearly resulting mainly from LIW (not WIW), and finally mixing  
22 with AW. During GIB2 (Fig. 4b), no violet profiles were observed. Instead, one relatively smooth  
23 blue profile tends to directly link AW and WMDW, with some bending due to lower-TDW, thus

1 clearly showing that dense MWs mix with AW far away from the sill, in the south and to depths of  
2 ~400 m at least (see Fig. 5). The orange and brown plots allow estimating the GIB1-GIB2  
3 differences (Fig. 4c; references to  $\theta$ -S diagrams a, b, c are, in general, not specified hereafter). Both  
4 LIW and TDW were more mixed during GIB2 than during GIB1, even though roughly the same  
5 WMDW was sampled at the densest levels. Note that  $\sigma = 29.08 \text{ kg.m}^{-3}$  can be used to separate, for  
6 the red and violet profiles, an upper irregular part associated with the light MWs from a lower  
7 smooth part associated with the dense MWs (this will be possible up to the sill).

8 The sections (Fig. 5) show that the northernmost profiles only indicate WIW. The WIW  $\theta_{\min}$   
9 is at 150-200 m (GIB1) and ~200 m (GIB2) while LIW is more clearly indicated by its  $S_{\max}$  at ~300  
10 m (GIB1) and 400-500 m (GIB2) than by its  $\theta_{\max}$  at ~200 m (GIB1) and ~300 m (GIB2). The WIW  
11 core is close to the upper slope, so that red profiles indicating mixed WIW are more to the south.  
12 Even though the LIW core (actually between  $\theta_{\max}$  and  $S_{\max}$ ) is also close to the northern slope, the  
13 LIW influence can reach the whole southern slope (GIB1) or only part of it (GIB2). As usual, TDW  
14 is never clearly indicated while WMDW is clearly indicated by its low  $\theta$ , relatively low S and high  
15  $\sigma$ . Below 500 m and at given depths, the TDW S and  $\theta$  values were higher during GIB1 than during  
16 GIB2. Even though  $\sigma$  was higher too, there was more TDW (vs. WMDW) during GIB1 than during  
17 GIB2. Also considering the relative amounts of WIW vs. LIW allows concluding that both light and  
18 dense MWs were more from the eastern basin during GIB1 and more from the western basin during  
19 GIB2.

## 20 2.2 The 5°00'W data

21 The shallowest GIB1 and GIB2 red profiles (Fig. 6) indicate that WIW is more mixed during  
22 GIB1, and some GIB1 (no GIB2) profiles only indicate little of it. General features for LIW are  
23 reversed, with LIW more mixed during GIB2. However, similar numbers of data representative of

1 WIW and LIW during GIB1 and GIB2 indicate similar amounts. All other GIB1 profiles were violet  
2 while only one violet profile was observed during GIB2 together with three blue ones. Note that  $\sigma$   
3  $>29.09 \text{ kg.m}^{-3}$  was found during GIB2 with some red, violet and blue profiles, but the largest values  
4 were blue even though the blue profiles were not the deepest ones (Fig. 7). S sections essentially  
5 show the LIW core at  $\sim 400$  m during GIB1 and GIB2 but the GIB1 LIW amount is larger than the  
6 GIB2 one.  $\theta$  sections show the WIW core at 100-200 m (GIB1) and 200-250 m (GIB2), together  
7 with the LIW core at 200-250 m (GIB1) and  $\sim 300$  m (GIB2). In the deeper part of the transects, the  
8 WMDW  $\theta_{\min}$  are relatively similar during GIB1 and GIB2 but they spread more southward up to  
9 400-500 m during GIB2. Consistently, largest GIB2  $\sigma$  also spread more southward so that deepest  
10 isopycnals start tilting up southward. Direct mixing between the dense MWs and AW is indicated  
11 down to  $\sim 400$  m (maximum depths) over nearly all the southern half of the GIB2 transect.

### 12 2.3 The $5^{\circ}15'W$ data

13 Since characteristics indicated by the red, violet and blue profiles at  $5^{\circ}15'W$  (Fig. 8) are not  
14 very different from those at  $4^{\circ}30'W$  (Fig. 4) and  $5^{\circ}00'W$  (Fig. 6), the MWs mixing does not  
15 markedly intensify along their westward route in the Alboran. The WIW amount is comparable  
16 (GIB1) or even larger (GIB2) than the LIW one. The S sections (Fig. 9) show more abundant and  
17 less mixed LIW during GIB1, cores having deepened to 400-500 m (deeper by 50-100 m than at  
18  $5^{\circ}00'W$ ) during both GIB1 and GIB2.  $\theta$  sections still show the WIW core at 100-200 m (GIB1) and  
19 200-250 m (GIB2), and the LIW core at 250-300 m (GIB1) and 300-350 m (GIB2), hence  $\sim 50$  m  
20 deeper than at  $5^{\circ}00'W$ . Lowest  $\theta$  and highest  $\sigma$  indicate that the densest MWs are found in the  
21 deeper part of the transect and tend to spread over the southern slope. Mixing of the dense MWs  
22 directly with AW is observed in the south down to  $\sim 600$  m.

### 23 2.4 The $5^{\circ}30'W$ data

1           The red profiles in Fig. 10 indicate WIW and LIW extrema as large, and even sometimes  
2 more pronounced, than at 4°30'W, confirming the reduced mixing of the light MWs downstream and  
3 the veins heterogeneity. The WIW amount is still comparable (GIB1) or even larger (GIB2) than the  
4 LIW one. The major differences with the profiles more to the east come from the violet and blue  
5 ones during GIB2 that tend to become AW-TDW and AW-WMDW mixing lines, respectively,  
6 which will appear to be a significant tendency. The very different shapes of nearby profiles, such as  
7 the two deepest red ones as well as the violet and the blue ones during GIB2, illustrate the difficulty  
8 of correctly sampling not only the light MWs cores but also the dense MWs. During GIB2, roughly  
9 the same dense MW sampled in the deepest parts of the red (at ~900 m; Fig. 11), violet (at ~700 m)  
10 and blue (at ~400 m) profiles spread over the deepest part of the southern slope. However, only its  
11 shallower/southernmost part (the blue profile) mixed with AW; note that the AW-TDW mixing at  
12 the nearby location (the violet profile) also reaches a maximum depth close to 400 m.

13           The LIW S core there is less clearly noticeable than more to the east, and it has markedly  
14 deepened along the slope during GIB1 while it has moved toward the strait central part during GIB2  
15 (Fig. 11).  $\theta$  sections still show the WIW core at 100-200 m (GIB1) and as deep as ~300 m (GIB2);  
16 they show the LIW core at 200-300 m (GIB1) and ~300 m (GIB2). Associating both the extrema  
17 amplitude and the relative areas occupied by WIW and LIW with the relative amounts of the two  
18 waters, the GIB1 and GIB2 data clearly illustrate an interaction between them along their westward  
19 route. During GIB1, the WIW amount is relatively low but WIW does not encounter major changes  
20 while the LIW amount is relatively large and LIW deepens, probably due to increasing velocities.  
21 During GIB2, the WIW amount is relatively large and WIW deepens while the LIW is relatively low  
22 and LIW is found away from the slope. Clearly, the larger the light MW amount, the larger its  
23 westward velocity and its tendency to deepen, due to rotation, and to push away the MW below, but

1 not modifying markedly the MW above. During GIB1 and GIB2, lowest  $\theta$  and highest  $\sigma$  occur in the  
2 south of this V-shaped passage where deep isolines tend to parallel the slope.

### 3 2.5 The 5°40'W data

4 Approaching the sill (just ~5 nm to the west), mixing intensifies markedly and leads to a  
5 relatively complex situation (Fig. 12). During GIB1, little amount of WIW is indicated on the  
6 available profiles down to ~100 m. Considering the amount and immersion of the WIW core more to  
7 the east, it might be that most WIW outflows more to the north. The four (out of six) red profiles  
8 show an AW-LIW mixing line while below, the LIW vein encounters marked disturbances. During  
9 GIB2, three (out of six) red profiles indicate that the WIW amount is still relatively large and that  
10 WIW  $\theta_{\min}$  are still in the 12.90-12.95 °C range, so that WIW can clearly be an important component  
11 of the MWs outflow. During GIB1, two violet profiles were straighter than previously, indicating an  
12 intensified AW-TDW mixing. During GIB2, none of the two violet profiles was as straight as at  
13 5°30'W while no violet profiles similar to the 5°40'W ones were observed at 5°30'W. A similar  
14 remark concerns the blue GIB2 profile that is not as straight as (or straighter than) at 5°30'W;  
15 differentiating it from the violet profiles was maintained as regard to continuity between the 5°30'W  
16 and 5°50'W data. The S distribution (Fig. 13) shows during GIB1 an LIW core still at 400-600 m,  
17 thus close to the deeper part of the strait there, and still along the slope while S values during GIB2  
18 are much lower and the core is still pushed away from the slope. The  $\theta$  distribution during GIB2  
19 indicates a large data amount in the 12.95-13.00 °C range at 200-300 m close to the northern slope,  
20 so that WIW actually represented a significant part of the outflow. The LIW  $\theta_{\max}$  is more marked  
21 during GIB1. The lowest  $\theta$  values, associated with the largest  $\sigma$  values, along the southern slope  
22 indicate both lower-TDW and WMDW, the latter during GIB2 only.

### 23 2.6 The 5°50'W data

1 Homogeneity of all profiles has increased, as expected 5 nm west of the sill, but marked  
2 north-south differences are still indicated. To emphasize the continuity with those more to the east,  
3  $\theta$ -S diagrams are first shown with the same scales (Fig. 14). Because the diagrams there are mainly  
4 mixing lines between some MW and AW, they were no longer colored according to their shape but  
5 according to the MW expected to be involved. Profiles involving either WIW or LIW are red while  
6 those involving TDW and WMDW are violet and blue, respectively. We also found more interesting  
7 to display in 14c the LYNCH data instead of the GIB1-GIB2 comparison, all being compared later  
8 on. LYNCH transects were performed twice, on both November 3 (LYNCH12) and 14 (LYNCH34),  
9 at locations roughly similar to the #1 (south) to #5 (north) GIB1 and GIB2 ones but the dramatic  
10 changes that occurred during the campaign prevent from a priori coloring the profiles.

11 Among the seven GIB1 profiles (Fig. 14a), the most straight and most southward one in the  
12 red group (#3) represents only AW-LIW mixing ( $\sigma_{\max} \sim 29.01 \text{ kg.m}^{-3}$ ) and does not indicate any  
13 WIW. Other ones, in particular the northernmost #6-7, indicate AW-WIW mixing only. The WIW  
14 signature on #4-5 accounts for the WIW importance even when in relatively low amount. The violet  
15 group (2 relatively close profiles,  $\sigma_{\max} \sim 29.03 \text{ kg.m}^{-3}$ ) indicates a similar AW-TDW mixing with few  
16 points near the #6-7 lower part. Even though the AW-WIW and AW-TDW mixing lines are partly  
17 superimposed, it is clear that the outflow is separated into three juxtaposed "suboutflows" that have  
18 markedly different  $\theta$ -S characteristics, maximum depth (see Fig. 17) and north-south location, the  
19 densest (respectively lightest) being the southernmost (respectively northernmost one). The  $\sigma_{\max}$   
20 associated with TDW and LIW differ by only  $\sim 0.02 \text{ kg.m}^{-3}$  and are larger by  $\sim 0.1 \text{ kg.m}^{-3}$  than the  
21 WIW one.

22 During GIB2 (Fig. 14b), which was characterized upstream by relatively large amounts of  
23 WIW vs. LIW and WMDW vs. TDW, a WMDW blue group (#1-2,  $\sigma_{\max} \sim 29.05 \text{ kg.m}^{-3}$ ) that is the

1 southernmost one is differentiated from a TDW violet group (#3-4,  $\sigma_{\max} \sim 29.025 \text{ kg.m}^{-3}$ ). Profile  
2 #5/GIB2 is extremely interesting since it shows a gap (28.911-28.945  $\text{kg.m}^{-3}$ ) and can thus be  
3 separated in two. Extrema reached by its deeper part are just slightly lower than the #3/GIB1 ones  
4 and thus indicate LIW, which is consistent with LIW during GIB2 more mixed than during GIB1.  
5 Extrema reached by its lower part correspond to the #6/GIB1 ones, hence accounting for the WIW  
6 importance also during GIB2. The GIB2 outflow was thus subdivided into four juxtaposed  
7 suboutflows, the interface between the WIW and LIW ones being inclined and intersected by #5 (see  
8 comments below about #6/GIB2). The  $\sigma_{\max}$  associated with WMDW, TDW and LIW differ from  
9 each other by only  $\sim 0.03 \text{ kg.m}^{-3}$  and are larger by 0.1-0.15  $\text{kg.m}^{-3}$  than the WIW one.

10 The four LYNCH transects (Fig. 14c) illustrate the tremendously large variability that can  
11 exist west of the sill just  $\sim 10$  days apart, mainly due to changes in the nature of AW (see 1.2.3). All  
12 LYNCH12 green profiles were relatively similar, in terms of rough location and slope, while the  
13 LYNCH34 cyan ones can be separated into a southern group (#1-2-3) and a northern one (#3-4-5),  
14 #3 belonging to one or the other group a few hours apart.

15 Comparing all diagrams in Fig. 14 allows two remarks. Within each group, mixing lines can  
16 be similar with markedly different  $\sigma_{\max}$  at markedly different depths (i.e. #1-2/GIB2; comparatively,  
17 #1-2/GIB1 reach less different depths). Since profiles nearly reached the bottom, this information  
18 demonstrates that the suboutflows are continuously stratified, the actual overall  $\sigma_{\max}$  occurring at  
19 greatest depths. Differences in  $\sigma_{\max}$  between groups during one campaign or for a group between the  
20 two campaigns can thus appear unreliable. However, plotting all diagrams together supports the  
21 profiles characterization and grouping we made (Fig. 15a). In particular, note that i) the WIW (pink)  
22 suboutflow is indicated by #6-7-(5)/GIB1 and #5-6/GIB2, ii) the LIW (red) one by #3-4-(5)/GIB1  
23 and #5/GIB2, iii) the TDW (violet) one by four indiscernible points (#1-2/GIB1 and #3-4/GIB2), iv)

1 the WMDW (blue) one by #1-2/GIB2 only. Also note that associated  $\sigma_{\max}$  increase from north  
2 (WIW) to south (WMDW) while the associated  $\theta$  decrease, and that the LYNCH grey dots  
3 concentrate around or tend toward GIB ones, which could allow coloring them accordingly.

4         The same  $\theta$ -S diagrams displayed over extended ranges (Fig. 16A for the MWs, Fig. 16B for  
5 AW) provide essential information and allow direct comparisons with the data downstream. First, all  
6 profiles in Fig. 16A are mixing lines between some AW and some MW. During GIB1 (Fig. 16Aa),  
7 profiles #1-2 (violet) and #3-4 (red) indicate different MWs (TDW vs. LIW) in their densest part and  
8 tend towards the same kind of AW while profiles #5-6-7 (red, mainly associated with WIW) tend  
9 toward another kind of AW. Similarly, during GIB2 (Fig. 16Ab), profile #3 is different from #1-2 in  
10 their densest part (WMDW vs. TDW) and becomes similar to them in their less dense part. Profile  
11 #6/GIB2 is now indicated and, due to both its similarities with the #5 upper part and its northernmost  
12 location, it is red and associated with WIW, which is consistent with the relatively large WIW-GIB2  
13 amount upstream. During LYNCH12, #1-2-3 and #4-5 form clearly different groups and the upper-  
14 part profiles tend to spread according to their north-south location. During LYNCH34, the two  
15 groups of profiles due to the MWs (#1-2-3 vs. #4-5) tend to form only one group upward. Note the  
16 similarities between the two groups of profiles during both GIB1 and GIB2 with either the  
17 LYNCH12 or LYNCH34 ones.

18         Figure 16B explains the upper-part profiles spreading indicated by Fig. 16A. Both NACW  
19 and SAW occurred, the latter displaying seasonal variations between spring (GIB1) and fall (GIB2,  
20 LYNCH). However, nearly opposed situations were encountered since during GIB1, SAW was  
21 mainly in the south (#1 to 4) and NACW mainly in the north (#5 to 7) while during GIB2, SAW was  
22 mainly in the north (#4 to 6) and NACW mainly in the south (#1 to 3). These variations of the  
23 NACW vs. SAW distributions in both time and space were observed along the other transects during  
24 both GIB1 and GIB2, which guarantees their significance. Even though such spatial variations have

1 never been mentioned and were unexpected, the temporal ones in the long-term (6 months apart for  
2 GIB) were less dramatic than the LYNCH ones in the short-term (Fig. 16Bc). During LYNCH, only  
3 NACW was present at the beginning (green) while only SAW was present at the end (cyan) ~10  
4 days after. As for GIB1 and GIB2, the LYNCH variations were observed as far as in the eastern  
5 Alboran. The marked changes that occurred during LYNCH in the composition of the MWs outflow  
6 east of the sill cannot be due to the changes in the distribution of NACW vs. SAW (Millot, 2008).  
7 Figures 16Ac and 16Bc demonstrate that the whole MWs outflow characteristics dramatically  
8 depend on the AW ones in the sill surroundings.

9         Figure 17 shows that the two violet GIB1 profiles and the two blue GIB2 ones were roughly  
10 at the same place, as were i) two red GIB1 profiles and the two violet GIB2 ones, ii) the red #5/GIB1  
11 (mixture of WIW and LIW) and #5/GIB2 (WIW above and LIW below). According to the available  
12 data, each of the four major MWs leads to a suboutflow during GIB2 while no suboutflow can be  
13 associated with WMDW during GIB1, consistently will all data upstream. The characteristics of the  
14 outflow can thus change dramatically at a given location/latitude, depending on the relative amounts  
15 of the MWs that, when present, are juxtaposed in the same way from north to south and mix  
16 individually with AW. The outflow is subdivided, as soon as 5°50'W, into a series of suboutflows  
17 that are associated with the MWs indicated upstream and are located side by side, the densest being  
18 the southernmost one. The southernmost profiles indicate the densest MWs along the lower part of  
19 the slope during both GIB1 and GIB2 since  $\sigma \sim 29.0 \text{ kg.m}^{-3}$  (representative of the MWs) tilts up  
20 southward while  $\sigma \sim 28.0 \text{ kg.m}^{-3}$  (the AW-MWs interface there) tilts up northward.

## 21         2.7 The 6°05'W data

22         The five profiles performed at 6°05'W during each campaign that were deep enough to  
23 possibly sample the MWs are displayed in both Fig. 18 and Fig. 15b, which allows comparisons with

1 those at 5°50'W in Fig. 16A and 15a. During GIB1, profile #1 is colored in violet and red since it is  
2 slightly but significantly different from the red group #2-3 that clearly indicates LIW while #4  
3 indicates WIW. As at 5°50'W and further upstream, no profile can be associated with WMDW.  
4 During GIB2, the associations #1-WMDW (note the undulated shape), #2-3-TDW and #4-WIW are  
5 clear, especially from Fig. 15b. No profile indicates LIW, which is consistent with the low amount of  
6 mixed LIW at 5°50'W and further upstream; as suggested by data downstream, the small LIW  
7 suboutflow was probably missed there. Similarly, and as demonstrated by the differences between  
8 #2 and #3 that both sampled the TDW suboutflow with inaccuracies similar to those already noticed  
9 at 5°50'W for #1-2/GIB2 (#3 is markedly deeper than #2), the WMDW suboutflow was not  
10 accurately sampled by profile #1 and must clearly be denser (in fact, the densest). Also note that  
11 #1/GIB1 did not correctly sample the TDW suboutflow and that there is a relatively large spacing  
12 between #1 and #2 during GIB2, which might indicate that the sampling interval there was not small  
13 enough. During LYNCH12, #2-3 indicate mixed LIW and #4 mixed WIW while during LYNCH34,  
14 consistent with the data at 5°50'W, #2 (performed in triplicate) once indicates WMDW, all other  
15 profiles indicating either more mixed WMDW or LIW.

16         The large spatial variability during all campaigns and the large temporal variability indicated  
17 by the LYNCH data illustrate the difficulty of correctly sampling there. Additionally, separating  
18 AW-MWs mixing lines for two different MWs depends on the nature of AW. For instance, NACW-  
19 TDW and NACW-WMDW lines are separated while the SAW-TDW and SAW-WMDW ones are  
20 superposed (the reverse occurs for WIW and LIW). It is thus obvious that a suboutflow can be either  
21 missed or mistaken with another one, and that the extrema are clearly depth dependent (those  
22 indicated by a unique-profile being unreliable). However, let us assume that the extrema associated  
23 with all the MWs during both GIB campaigns (except WMDW not correctly sampled during GIB2)  
24 are representative of the actual ones. Even though the outflow composition during GIB1 (WIW,

1 LIW, TDW, no WMDW) and GIB2 (WIW, little LIW, TDW, WMDW) was markedly different,  
2 each of the MWs was characterized by extrema that were shifted from 5°50'W to 6°05'W along the  
3 mixing lines with AW, which supports the coloring. The  $\sigma_{\max}$  shift is  $\sim 0.1 \text{ kg.m}^{-3}$  for TDW and LIW,  
4  $\sim 0.2 \text{ kg.m}^{-3}$  for WIW. Note that  $\Delta\sigma_{\max}$  between the two densest suboutflows (TDW and LIW during  
5 GIB1, WMDW and TDW during GIB2) differ by  $0.1\text{-}0.2 \text{ kg.m}^{-3}$  while the range for all MWs is  
6  $\Delta\sigma = 0.2\text{-}0.3 \text{ kg.m}^{-3}$  (associated with  $\Delta\theta = 0.2\text{-}0.3 \text{ }^\circ\text{C}$ ,  $\Delta S = 0.2\text{-}0.3$ ). Ranges at a given location for the  
7 densest suboutflows (between TDW-GIB1 and WMDW-GIB2 or between LIW-GIB1 and TDW-  
8 GIB2) are about half these values. Even though characterizing a priori a given suboutflow by  
9 specific hydrographic values corresponding to a given MW is impossible, the southernmost  
10 (respectively northernmost) suboutflow expected to be actually the denser (lighter) might always be  
11 relatively cool (warm), compared to the neighboring ones, which would correspond to the  
12 observations about the veins downstream. Assuming a homogeneous outflow was certainly  
13 hypothesized for convenience but has never been supported by any data set, and no data sets is more  
14 detailed or can be considered as more reliable than the GE one, even if still not accurate enough.

15 GIB1 and GIB2 are not very informative about the densest/southernmost suboutflow (Fig.  
16 18) that is indicated by only one (#1) non-very representative profile. Overall largest densities were  
17 certainly missed: during GIB1, they were due to TDW and thus probably south of #1 since #1 is still  
18 relatively similar to #2-3 that indicate LIW; during GIB2, they were due to WMDW and thus  
19 probably between #1 and #2 since corresponding depth must be greater than at #1. During both  
20 LYNCH12 and LYNCH34, the densest/southernmost suboutflow is indicated by profiles #2 mainly  
21 since #1 is either out of range or indicative of more mixed water while #3-4 indicate either the same  
22 MW more mixed or another MW. We thus expect this suboutflow and other ones as well to have  
23 moved toward the central part of the transect, which is somehow supported by the sections (Fig. 19).  
24 Apart from the NACW intrusion at 200-250 m during GIB2 (leading to the undulations on #1, Fig.

1 18), and even though overall maximum densities associated with the southernmost / densest  
2 suboutflow were certainly missed, the deep isopycnals tend to flatten (GIB1) or even to tilt up  
3 northward (GIB2).

#### 4 2.8 The 6°15'W data

5 Among the four/eight GIB1/GIB2 profiles (Fig. 20), only two/three of the profiles sampled  
6 the outflow now found in the lower part of the northern/Iberian continental slope, which confirms  
7 the displacement of the densest MWs from the southern slope (~5°50'W) to the central part of the  
8 strait (~6°05'W) and finally to the northern slope (~6°15'W). Such a limited number of profiles does  
9 not allow statistically significant results but they provide extremely valuable information. Since the  
10  $S_{\max}$  found at 400-600 m near 6°30'W is  $S \sim 37$  (Borenäs et al., 2002), we focus on larger values.  $\theta$ -S  
11 diagrams (Fig. 21) are no longer straight mixing lines and display marked undulations. These major  
12 changes prevent coloring the profiles as done upstream but, more interestingly, several comments  
13 support coloration by undulation.

14 A mid-depth undulation such as the bump identified by a continuous line on the #6/GIB2  $\theta$ -S  
15 diagram (Fig. 21b) indicates  $\theta$  and S relative maxima. This bump's general shape is similar to that of  
16 any diagram displaying LIW in the sea or the whole outflow in the ocean so that it characterizes an  
17 intermediate vein of relatively warm salty water. Other mid-depth bumps that do not have relative  
18 maxima depict a more mixed vein, or at least intrusions, of MWs into AW. Successive bumps on a  
19 given diagram thus indicate overlying veins or intrusions that are supposed contiguous. The lowest  
20 parts of the #3/GIB1 and #5-6-7/GIB2 diagrams are markedly bended and represent the upper part of  
21 such bumps. Because profiles covered nearly all the water column, these half-bumps indicate actual  
22 veins still flowing over the bottom.

1 We assume that i) the suboutflows upstream (at 5°50'W (Fig. 16A) and 6°05'W (Fig. 18)),  
2 which are consistent with the MWs amounts east of the sill, cascade individually and lead to specific  
3 veins at 6°15'W, ii) all significant suboutflows upstream and veins at 6°15'W were sampled so that  
4 each MW presence / absence is consistent in the whole study area, iii) the suboutflows and veins  
5  $\sigma_{\max}$  are not accurately defined, in particular with only one profile, and the densest suboutflow  
6 (respectively vein) is the southernmost (respectively deepest) one, iv) veins flow along the northern  
7 slope at 6°15'W, as expected for any density current (Fig. 20), v) when sampling a warm salty vein  
8 with profiles approaching its core, all characteristics ( $\theta$ , S and  $\sigma$ ) regularly increase, so that links  
9 exist between bumps on neighboring profiles (Fig. 21). The quite satisfying coloration we came with  
10 is: WIW (pink) during GIB1 and GIB2, LIW (red) mainly during GIB1 and both mixed and in small  
11 amount during GIB2, TDW (violet) during both GIB2 and GIB1, WMDW (blue) during GIB2 only.  
12 When comparing GIB1 and GIB2, a major remark concerns the TDW  $\sigma_{\max}$ . During GIB1, TDW is  
13 the densest vein and its  $\sigma_{\max}$  reduces only slightly (by  $\sim 0.2 \text{ kg.m}^{-3}$ ) from 5°50'W (where it is well  
14 defined) to 6°15'W, roughly as much as the WMDW  $\sigma_{\max}$  during GIB2 (reducing  $\sim 0.25 \text{ kg.m}^{-3}$ ).  
15 During GIB2, TDW is no more the densest vein and its  $\sigma_{\max}$  reducing is larger (by  $\sim 0.5 \text{ kg.m}^{-3}$ ). A  
16 similar remark concerns the LIW  $\sigma_{\max}$  that reduces only by  $\sim 0.5 \text{ kg.m}^{-3}$  when unmixed and in large  
17 amount (GIB1) and by  $\sim 0.7 \text{ kg.m}^{-3}$  when mixed and in small amount (GIB2). The WIW  $\sigma_{\max}$   
18 reduced by larger amounts. Overall and as expected, the mixing of a vein with AW is inversely  
19 proportional to its depth an amount: the greater the depth and amount, the lower its  $\sigma_{\max}$  reducing.

20 The colored bars in Fig. 20 confirm these hypotheses since the pink, red, violet and blue  
21 layers have realistic thicknesses and mean depths on the various profiles during both GIB1 and  
22 GIB2. The non-occurrence of any red-LIW bump on #4/GIB1 that would be expected from the #3  
23 bump leads to a relatively thick pink layer there, which might be due to small-scale heterogeneity.  
24 The #7/GIB2 red-LIW half-bump is not retrieved on #5-6, which is consistent with the LIW/GIB2

1 small amount. Quite surprisingly, both WIW and TDW that were almost never mentioned in current  
2 thoughts (subsection 1.1) represented large percentages of the outflow during both GIB1 and GIB2.  
3 Quite surprisingly too, LIW and WMDW that are currently thought as being the sole components of  
4 the outflow can represent a low percentage (LIW during GIB2) or be absent (WMDW during GIB1).

5 Figure 21 shows that the two densest veins  $\sigma_{\max}$  (GIB1: TDW and LIW, GIB2: WMDW and  
6 TDW) differ by a similar  $\Delta\sigma_{\max} \sim 0.3 \text{ kg.m}^{-3}$  even though the GIB1- $\sigma_{\max}$  are slightly larger than the  
7 GIB2- $\sigma_{\max}$  ones. Since this difference at  $6^{\circ}15'W$  corresponds to those reported 100-200 km  
8 downstream when the veins no longer cascade and are characterized by  $\sigma_{\max}$  lower by  $\sim 1.0 \text{ kg.m}^{-3}$ , it  
9 might be that the densest veins similarly mix downstream. Even though the densest veins correspond  
10 to different MWs, the deep vein is  $\sim 90\text{-m}$  thick and the intermediate one is  $50\text{-m}$  thick during both  
11 GIB1 and GIB2. Furthermore the two veins have roughly similar  $\theta$  and S even though associated  
12 with different MWs, this clearly explains the permanency of the veins characteristics currently  
13 assumed. The third upper vein described in the literature is the WIW vein (possibly confused with  
14 the LIW one as during GIB2), it is consistently the warmest, and  $\Delta\sigma_{\max}$  are within the reported  
15 ranges.

16 During GIB1, the S section (Fig. 20) also shows the AW  $S_{\min}$  ( $<36.0$ ) spreading over the  
17 whole transect. The low  $\theta$  values at the base of the southern/Moroccan slope indicate NACW and  
18 some relative maxima over the northern slope indicate heterogeneities due to the AW-MWs  
19 interactions, while all densest isopycnals are tilting up northward. During GIB2, the AW  $S_{\min}$  is less  
20 spread and the MWs  $S_{\max}$  values are slightly lower. The  $\theta$  section still indicates NACW, which  
21 might be a frequent (if not permanent) feature, together with numerous heterogeneities.

22

### 1           3. The 80-m and 270-m time series analysis

2           The HCP data are presented in subsection 1.2. Major results concerning the composition and  
3 spatio-temporal variability of the MWs outflow are displayed with a series of  $\theta$ -S diagrams allowing  
4 comparisons between the data at both locations over time. The number of diagrams/periods (six for  
5 the 2003-2007 time series) is a compromise allowing a relatively large number of diverse situations  
6 to be differentiated (Fig. 22). The selection made from a visual analysis only is validated by the large  
7 variability. As expected from the GE transects analysis, only LIW, TDW and WMDW (not WIW)  
8 were found at the sill and/or on the Moroccan shelf, so that only the upper part (38.44-38.52) of the  
9 MWs S-range is of interest. Similarly, the MWs  $\theta$ -range is reduced to 12.92-13.25 °C since i) the  
10 lowest  $\theta$  are generally located along the Moroccan slope, i.e. neither at the sill nor on the shelf, ii)  
11 marked changes have occurred in the sea, and/or iii) the oceanic trends are generally positive.  
12 Because TDW i) cannot be clearly differentiated from LIW above and WMDW below, ii) is not  
13 characterized by any extremum and iii) is often encountered at 270 m, terms such as lower, central  
14 and upper parts of a unique TDW-range (on such diagrams) are used to deal, as precisely as possible,  
15 with TDW being more or less dense (over time). Both NACW and SAW were measured at 80 m (not  
16 shown). Days are Julian days from January 1<sup>st</sup>, 2003, and successive periods are separated by 20  
17 days to avoid confusing situations.

18           Days #12-450 (Fig. 22a). At 270 m, relatively high  $\sigma$  (29.095-29.100 kg.m<sup>-3</sup>) and S,  
19 associated with either TDW or LIW, occurred during this period (blue points). This is particularly  
20 obvious when TDW unmixed with either AW or any other MW was continuously observed during  
21 the three first days (gold), so that more extreme situations probably occurred before. Even though  
22 this was during neaps (subsection 4.1), this suggests a relatively intense TDW outflow. As shown by  
23 several dashed lines nearly parallel to isopycnals >29.08 kg.m<sup>-3</sup> for central-TDW (also for upper-

1 TDW and LIW, unclear in the figure), MWs unmixed with AW were often observed during several  
2 consecutive records. However, mixing with AW (lines nearly perpendicular to the isopycnals) due to  
3 the internal tide was generally significant at the sill (even when the most homogeneous LIW  
4 outflowed), hence for the whole MWs outflow. No points indicative of either lower-TDW or  
5 WMDW were observed during this 440-day period. At 80 m, points (cyan) were very rare (they were  
6 never so rare thereafter) and they all indicated intense mixing with AW. Compared to points at 270  
7 m, points at 80 m were generally more shifted toward the lower left part of the diagram, which is a  
8 80-m vs. 270-m difference often encountered hereafter. Links exist between the MWs found at both  
9 locations and between the facts that large densities occurred at the sill when few MWs occurred on  
10 the shelf.

11 Days #470-670 (Fig. 22b). At 270 m (green), either LIW or upper- and central-TDW were  
12 still encountered, sometimes not mixed with AW during several consecutive records but now with  
13 markedly lower S. Values at 80 m (yellow) were sometimes denser than at 270 m, still associated  
14 with either LIW or TDW but in less mixed conditions. Compared to those during the twice-longer  
15 period #1, 80-m points were more numerous. But similarly, 80-m points were more shifted towards  
16 cooler and fresher waters than 270-m ones. Points signed mainly TDW (upper, central and lower) at  
17 80 m, and mainly LIW and upper + central (lower is rare) TDW at 270 m. Links exist between  
18 relatively light MWs at the sill and much denser MWs on the shelf.

19 Days #690-790 (Fig. 22c). Only LIW, more or less mixed with AW, was found at 270 m  
20 (red) with  $\theta$  and S values significantly lower than during the two previous periods while only LIW  
21 (and/or upper-TDW) more mixed with AW was found at 80 m (pink). Since the densest waters  
22 (lower-TDW and WMDW), generally located along the Moroccan slope, were not sampled at any  
23 place, they were either absent or present in a limited amount. Such a situation, with no (observed) or

1 little (possibly outflowing) dense MWs from either the eastern basin (TDW) or the western one  
2 (WMDW), has never been encountered since.

3 Days #810-870 (Fig. 22d). Dramatic changes have now occurred at both 270 m (brown) and  
4 80 m (violet). At 270 m, upper- to lower-TDW and rare WMDW were found in relatively unmixed  
5 conditions, as indicated by the low number of AW-TDW and AW-WMDW mixing lines as  
6 compared to the number of lines roughly parallel to the isopycnals (clear at least for upper-TDW).  
7 At 80 m, mainly WMDW and lower- to central-TDW were found in more mixed (less salty at least)  
8 conditions. From the beginning of the experiment, it is the first time that no LIW was recorded, that  
9 lower-TDW was relatively frequent, and that WMDW was present at both locations, which indicates  
10 an outflow mainly of western origin. The mainly eastern origin has lasted for ~800 days at least,  
11 probably more since the situation at the beginning of the experiment was relatively extreme.

12 Days #890-1140 (Fig. 22e). The situation markedly changed again since now all three MWs  
13 (LIW, TDW and WMDW) were measured at both 270 m (dark green) and 80 m (light green). They  
14 were mixed either together (clear for lower-TDW and WMDW) or with AW at 270 m while there  
15 were mixed only with AW at 80 m. Characteristics of both LIW and upper-TDW at 270 m were less  
16 extreme (warm and salty) than during period #1 (and #6), but together with the characteristics of the  
17 lower-TDW, they were more pronounced (saltier at least) than during periods #2-3-4. Most of the  
18 MWs at 80 m can be considered as a mixture of those at 270 m. But as during period #4, the coolest  
19 values sign WMDW never found at 270 m.

20 Days #1160-1536 (Fig. 22f). Period #6 at 270 m (brown) is characterized by upper-TDW  
21 similar to that encountered during period #1, and by central- to lower-TDW more abundant and even  
22 denser ( $<29.104 \text{ kg.m}^{-3}$ ) than during period #1, together with less LIW and more WMDW. At 80 m  
23 (orange), mainly WMDW, central- and lower-TDW occurred. Note that, overall, the less mixed (i.e.

1 densest) central- to lower-TDW (at 270 m) and WMDW (at 80 m) were observed simultaneously  
2 during this period.

3 Days #1536-1760 (not shown). Even though the CTDs used from March 2007 to October  
4 2008 are not post-calibrated yet, the continuity of the time series from before to after day #1556  
5 accounts for the accuracy of the data shown in Fig. 22f in particular. During this 220-day period,  
6 data at 270 m suggest the occurrence of upper- to lower-TDW as in Fig. 22d and Fig. 22e while data  
7 at 80 m in the displayed ranges are even more rare than in Fig. 22a. Assuming corrections similar to  
8 those previously made would not dramatically change these features, which would illustrate another  
9 situation never encountered up to now.

10

#### 11 4. Discussion

12 Complementary analyses provide a more detailed description of the MWs outflow. A current  
13 meter at 270 m allows specifying some aspects of its short-term variability (4.1). Statistics on the 4-  
14 year long time series at 270 m provide significant information on its seasonal variability (4.2). A  
15 synthesis of the results obtained with the time series at both 80 m and 270 m allows specifying its  
16 long-term variability (4.3). The low mixing of the light MWs up to the sill and the continuous  
17 evolution of the outflow structure meanwhile allow simple computations that explain some of the  
18 current thoughts and quantify the GIB1 vs. GIB2 differences (4.4). Finally, a new concept of the  
19 MWs outflow is proposed with the major aim to motivate as many as possible further studies (4.5).

#### 20 4.1 Short-term variability

21 A RCM9 Aanderra current meter set at 270 m worked for ~6.5 months in early 2003. One-  
22 hour velocities (V), all measured in the 225-45°T direction, ranged from +190 cm.s<sup>-1</sup> (towards

1 225°T) to  $-135 \text{ cm.s}^{-1}$  due to the large semi-diurnal variability. The daily (25-h) moving average of V  
2 (Fig. 23) displays a well-known (Candela et al., 1990) fortnightly signal locked on the tide at Tarifa  
3 with maximum deep-sill current during neaps, which is consistent with the largest outflow at springs  
4 (Bryden et al., 1994; Vargas et al., 2006). The CTD data allow plotting  $\sigma$  as grey and cyan dots, the  
5 latter resulting from a selection based on a criterion explained in subsection 4.2. The S (38.32-38.51)  
6 and  $\theta$  (13.0-13.25 °C) curves are almost identical (S) or similar ( $\theta$ , descending axis) to the  $\sigma$  one.

7 The  $\sigma$  and V curves are in phase, the densest less-mixed MWs rapidly outflowing during  
8 neaps. During days #12-14, the largest  $\sigma$  measured at the beginning of the experiment (Fig. 22a, gold  
9 points) lead to daily averages  $>29.096 \text{ kg.m}^{-3}$ , and V was the largest ever measured too ( $\sim 120 \text{ cm.s}^{-1}$   
10 on day #13, 4-day average  $\sim 100 \text{ cm.s}^{-1}$ ). Such a rapid outflow of dense MWs, even if maybe of  
11 limited vertical extent, probably represented a significant part of the whole outflow. Near day #80,  
12 the lowest  $\sigma$  ( $\sim 28.90 \text{ kg.m}^{-3}$ ) were associated with the lowest V ( $\sim 25 \text{ cm.s}^{-1}$ ), such a slow outflow of  
13 relatively light MWs probably not significantly modifying the whole outflow. Note that no  $\sigma$  values  
14 were selected at this time by the criterion. The huge fortnightly variability of the hydrographic  
15 parameters at the sill is obviously larger at shallower depths across the whole strait, which leads to a  
16 significant signal all along the outflow downstream that has never been looked for.

17 During this 6.5-month period, and even though variations induced on both  $\sigma$  and V by the  
18 tide and other unknown or unresolved forcings are relatively large,  $\sigma$  data selected for the MWs  
19 were still in a relatively high range (29.05-29.10  $\text{kg.m}^{-3}$ ) while the overall mean V =66 cm/s, which  
20 is a relatively large value as compared to other published ones (e.g. Bryden et al., 1994). These  
21 features are used to explain the differences we make thereafter between an overflow and an outflow.

## 22 4.2 Seasonal variability

1           We do not expect any seasonal variability of the MWs outflow up to the sill (see 1.2),  
2   contrary to what occurs for the AW inflow (Millot, 2007). The 4-year long and 1-h time series  
3   (36600 data) at 270 m, where points representative of the MWs are more numerous and less  
4   dependent on tidal mixing than at 80 m, allows some objective and probably significant analysis. We  
5   address the seasonal variability first with a standard fitting of the 270-m time series, then with a  
6   method we are elaborating and already applied to the 80-m one (Millot, 2007).

7           The curves in Fig. 24 represent the polynomial fits to sets of  $\theta$ ,  $S$  and  $\sigma$  data selected in  
8   different ways for each of the four years starting in January 2003. The polynomial degree (three) and  
9   1-year periods are a priori able to detect any almost regular/sinusoidal signal. The black curves are  
10   for all points in the MWs ranges used for Fig. 24 (38.44-38.52, 12.90-13.25 °C, 29.06-29.10 kg.m<sup>-3</sup>),  
11   which selects numerous points indicative of AW-MWs mixing. The red curves are from points  
12   selected according to a tidal criterion, i.e. retaining only the  $\theta_{\min}$ ,  $S_{\max}$  and  $\sigma_{\max}$  for each consecutive  
13   semi-diurnal (12-h) period, which gives 3050 regularly distributed points that can still be influenced  
14   by AW-MWs mixing, particularly during springs. The blue curves are from the sets of 3050 points  
15   selected according to a standard deviation (sd) criterion. A sd being computed over some (three)  
16   consecutive data and associated with the central one, only the data for which the sd is lower than  
17   some arbitrarily-fixed maximum value are retained, which allows selecting data representative of the  
18   most homogeneous MWs at one's convenience.

19           For all three parameters, relatively similar "seasonal" variations are observed during years  
20   #1-2 on one side, and during years #3-4 on the other side. The former are very different, if not  
21   opposed, to the latter. The corrected time series ending in March 2007, we did the same analysis  
22   over four years with a 2-month shift, as well as over three years with a 6-month shift. We also  
23   conducted similar analyses with the 80-m time series. All three time-intervals lead to the same

1 conclusion at both 80 and 270 m, i.e. that  $S$ ,  $\theta$  and  $\sigma$  for the MWs do not show any kind of seasonal  
2 variability.

3         Interesting information is provided by the distribution with time of the data selected with the  
4 sd criterion. Relatively unmixed AW and MWs being defined by specific ranges (AW:  $S < 37$ ,  $\theta$   
5  $> 13.5$  °C; MWs:  $S > 38.4$ ,  $\theta < 13.25$  °C), frequencies of occurrence for both waters are about 67%  
6 and 8% at 80 m, 0% and 92% at 270 m. One can then consider, for both AW and the MWs, the  
7 distribution with time (1-month averages) of the most homogeneous data (i.e. having the lowest sd;  
8 we arbitrarily chose the 30% most homogeneous) in  $S$ ,  $\theta$  and  $\sigma$ , as well as of the so-called triplets  
9 that correspond to the sets of data selected at the same time for all three parameters. Considering  
10 other realistic ranges for either AW or the MWs, and/or computing the sd over two or four  
11 consecutive values, and/or selecting slightly more (i.e. 40%) or less (i.e. 20%) homogeneous data  
12 does not basically change the results displayed in Fig. 25.

13         For the AW at 80 m (Fig. 25a), the distribution with time of the 7320 data (30% of 67% of  
14 the 36600 available data) selected for all three parameters, and of the 4437 triplets that result from  
15 this selection, displays a marked seasonal variability. Most homogeneous data and numerous triplets  
16 occur during the second half of February (dashed lines). This is linked to the meteorological  
17 conditions in the study area and the wintertime mixing of any surface layer that leads to the  $S$ (AW)  
18 seasonal variability (Millot, 2007). As confirmed by a sharper selection (i.e. less than 30%) the  
19 interannual variability is significant too.

20         For the MWs at 80 m (Fig. 25b), the distribution of the 915 data (30% of 8%) and of the 695  
21 triplets displays marked seasonal and interannual variabilities. The seasonal variability appears as a  
22 peak occurring well after the AW peak, i.e. when AW starts re-stratifying and no longer mixes with  
23 the MWs as during the winter, allowing unmixed MWs to be often sampled. Then, seasonal

1 stratification reaches the MWs layer and lowers the number of homogeneous data. The interannual  
2 variability mainly shows the non-occurrence in 2003 and the rare occurrence in early 2004 of the  
3 MWs (Fig. 22a). The similarity between the curves for the three parameters yields to a relatively  
4 large number of triplets not related to some specific character of the MWs there. Rather, the scarcity  
5 of unmixed MWs leads to select data influenced by mixing with AW, hence distributed, in a  $\theta$ -S  
6 diagram, along lines roughly perpendicular to the isopycnals. Standard deviations for all three  
7 parameters are thus proportional, leading data to be selected at the same time. The large interannual  
8 variability prevents from evidencing the seasonal variability with a polynomial fit.

9 For the MWs at 270 m (Fig. 25c), the distribution of the 10980 data (30% of 92%) and of the  
10 5651 triplets displays a marked interannual variability (see 4.3) with no seasonal variability. This is  
11 obviously representative of most of the outflow approaching the sill. However, tidal mixing with  
12 AW at the sill is intense (e.g. Fig. 22-23), characteristics of the outflow downstream from the sill  
13 markedly depend on AW in the sill surroundings (e.g. Fig. 18c) and AW displays a marked seasonal  
14 variability (Fig. 25a). Therefore, the MWs outflow in the ocean should display a seasonal variability  
15 imposed, via mixing with AW in the sill surroundings, by the meteorological forcing.

#### 16 4.3 Long-term variability

17 Figure 25c also indicates that the three parameters at 270 m have non-related variations and  
18 relatively similar and constant mean levels in 2003-2004 while they have larger and sometimes more  
19 similar variations with different levels in 2005-2006. The MWs in 2003-2004 were more  
20 homogeneous in S and  $\theta$  than in  $\sigma$  while, in 2005-2006, they were more homogeneous in  $\sigma$  than in S  
21 and  $\theta$ , which is related to the general shape of the  $\theta$ -S diagrams (Fig. 22) that were more aligned  
22 with the isopycnals during the second half of the experiment. The large number of homogeneous  $\theta$  at

1 the end of 2004 corresponds to period #3 with only LIW (Fig. 22c). The simultaneity of some 270-m  
2 peaks in 2005 might be fortuitous since they are not simultaneous in 2006.

3         Considering the LIW and upper-TDW vs. WIW amounts, as well as the lower-TDW vs.  
4 WMDW ones, the GE data show that the outflow can be more of eastern (GIB1) or western (GIB2)  
5 origin. Consistently, blue profiles (Tab.1) were never observed during GIB1 while observed on all  
6 transects during GIB2. Both campaigns also show that, in the sill surroundings, the MWs are more  
7 juxtaposed than superposed, the denser further south, and that all MWs mix more with AW than  
8 together. Finally, the light-dense MWs interface ( $\sigma = 29.08 \text{ kg.m}^{-3}$ , Fig. 3) markedly tilts east of the  
9 sill, up to being nearly parallel to the southern continental slope, during both GIB1 and GIB2. Such  
10 information about the outflow long-term variations and cross-strait distribution currently inferred  
11 from CTD profiles is fully consistent with that inferred from the less standard CTD time series.

12         Before comparing the six periods defined for the 2003-2007 HCP experiment (Fig. 22), some  
13 points must be specified. Time series at 80 m on the Moroccan shelf and at 270 m near Camarinal  
14 Sill South do not generally indicate the densest MWs that are expected (from e.g. the GE data) to be  
15 at 200-300 m along the Moroccan slope. Such time series do not provide information about WIW  
16 that always outflows more to the north at shallower depths. The LIW  $S$  and  $\theta$  overall maxima in  
17 2003-2007 at 270 m and  $5^{\circ}45'W$  ( $>38.51$ ,  $>13.15$  °C) were encountered ~20 years ago in the western  
18 Alboran but never expected to be measured at the sill (Millot et al., 2006). A 1984 one-week time  
19 series at the sill (294 m; Pettigrew, 1989), i.e. close to our 270-m site, regularly indicated  $\theta < 12.9$   
20 °C, hence relatively unmixed WMDW, while we measured only ~100 values out of ~36600 in a  
21 higher range of 12.92-12.95 °C and only during the second half of the experiment.

22         Main characteristics during period #1 (~440 days, Fig. 22a) are the occurrence of relatively  
23 large densities at 270 m associated with TDW (not WMDW) and the scarcity of points at 80 m

1 mainly showing mixed TDW (not WMDW). This makes unlikely the outflow of a significant  
2 amount of WMDW along the slope in between. When considering the large speeds at 270 m, we  
3 expect (without any proof) the isopycnals to have been either horizontal or tilting up northward.  
4 Such a situation illustrates what we call an overflow.

5 An almost opposite situation occurred during period #2 (~200 days, Fig. 22b) with relatively  
6 low densities at 270 m, associated with either LIW or TDW, and relatively numerous points at 80 m  
7 sometimes indicating either LIW or TDW denser than at 270 m. There is little chance of finding a  
8 WMDW outflow in between. However, denser TDW was certainly outflowing along the slope since  
9 AW-MWs mixing is lower there than on the shelf. Such a situation indicating a relatively large  
10 tilting up of the MWs isopycnals southward is the most extreme we encountered.

11 Another extreme situation occurred during period #3 (~100 days, Fig. 22c) with only  
12 relatively mixed LIW at both 270 and 80 m, hence probably leaving no place in between for some  
13 TDW or WMDW outflow. One can think either that a core of less mixed LIW is outflowing more to  
14 the north, making LIW the dominant component of the outflow, or that a relatively large amount of  
15 WIW is outflowing too, hence pushing the LIW core away from the northern slope, as during GIB2.

16 Dramatic changes then occurred since no LIW at all was observed at either 270 or 80 m  
17 during period #4 (~60 days, Fig. 22d). Instead, relatively unmixed, although relatively light, TDW  
18 was observed at 270 m while waters at 80 m were either similar, even if more mixed, to those at 270  
19 m or markedly different indicating for the first time the occurrence of mixed WMDW there, and  
20 hence the possible occurrence of less mixed WMDW along the slope in between. During period #5  
21 (~250 days, Fig. 22e), similar comments can be made about TDW and WMDW at both 270 and 80  
22 m. But LIW was also often encountered at both sites in more or less mixed conditions. Denser  
23 WMDW might have outflowed along the southern slope. During period #6 (~380 days, Fig. 22f) the

1 LIW occurrence markedly reduced at 270 m and completely disappeared at 80 m. The overall  
2 densest TDW and maybe some WMDW were encountered at 270 m while the overall less-mixed  
3 WMDW was observed at 80 m, hence suggesting that denser WMDW were significantly outflowing  
4 in between.

5 The alternation of a MWs outflow mainly originated from either the western basin or the  
6 eastern one as suggested by the GE profiles is thus definitely demonstrated by the HCP time series  
7 that, additionally, document the large variability in all MWs amounts. Moored CTDs, possibly  
8 complemented by ship-handled CTDs operated along transects as often as possible, are clearly  
9 efficient, reliable and relatively simple instruments that are suitable for monitoring strategies and can  
10 provide significant information about such an outflow composition and variability in the long-term.

#### 11 4.4 A two-layer approximation up to the sill

12 This subsection aims at checking, with relatively crude computations from the GE data, if  
13 differentiating light vs. dense (instead of intermediate vs. deep) MWs, can help explaining some of  
14 the current thoughts (such as the 90% LIW and 10% WMDW). Another aim is to help us better  
15 describing how a MW such as WMDW can reach the sill depth, hence to try improving our own  
16 understanding of the whole sea functioning.

17 The GIB data set indicates that, from east to west in the Alboran up to the sill, the mixing of  
18 all MWs does not especially increase while all associated isopycnals more and more tilt up  
19 southward. Close to the sill, let's say from  $\sim 5^{\circ}15'W$  to  $\sim 5^{\circ}40'W$ , it can be easily assumed that both  
20 the light MWs (WIW, LIW, upper-TDW) and the dense MWs (lower-TDW, WMDW) circulate  
21 significantly all across the strait, even if more or less homogeneously. More to the east, i.e. from  
22  $\sim 4^{\circ}30'W$  to  $\sim 5^{\circ}00'W$ , this is expectedly not the case since, according to our personal thoughts, dense  
23 MWs are quite motionless while, according to our data analysis, they can be found just below AW in

1 the south. The thermal wind equations for two homogeneous layers can thus be used to check if  
 2 assuming an outflow composed of two (sets of) MWs as done by previous authors is supported by  
 3 the GE data or not. When characterizing the light vs. dense MWs by mean values of density ( $\rho_L$  vs.  
 4  $\rho_D$ ), speed ( $V_L$  vs.  $V_D$ ) and amount, i.e. section area ( $A_L$  vs.  $A_D$ ), the slope of their interface is:

$$5 \quad I_{LD} = f/g/(\rho_D - \rho_L) \cdot (\rho_D V_D - \rho_L V_L)$$

6 with  $f$  the Coriolis parameter ( $10^{-4} \text{ s}^{-1}$ ) and  $g$  gravity ( $10 \text{ m.s}^{-2}$ ),  $I_{LD} < 0$  indicating a tilting up  
 7 southward. These mean values must also satisfy the relationship:

$$8 \quad V_L A_L + V_D A_D = Q$$

9 with  $Q$  the outflow transport. Specifying  $\rho$  values from the GE data (as displayed in particular by the  
 10  $\theta$ - $S$  diagrams),  $A$  values from e.g. Fig. 3, and  $Q$  from the literature allows computing  $V_L$  and  $V_D$   
 11 values, hence checking the light vs. dense MWs transports ( $Q_L = V_L A_L$  vs.  $Q_D = V_D A_D$ ).

12 We chose  $\rho_L = 1\,029.05 \text{ kg.m}^{-3}$  and  $\rho_D = 1\,029.09 \text{ kg.m}^{-3}$ . We specified  $A_L$  and  $A_D$  from  
 13 interfaces defined by  $\rho_{LD} = 1\,029.08 \text{ kg.m}^{-3}$  for the light-dense MWs interface (slope =  $I_{LD}$ ) and  $\rho_{AM} = 1$   
 14  $028.75 \text{ kg.m}^{-3}$  for the AW-MWs interface. We retained for  $Q$  the most recent and generally accepted  
 15 estimate of  $0.7 \cdot 10^6 \text{ .m}^3 \cdot \text{s}^{-1}$  (Bryden et al. 1994). These assumptions and estimates are very crude but  
 16 we checked what could be foreseen from the equations, i.e. that modifying realistically these values,  
 17 hence changing  $Q_L$  vs.  $Q_D$ , does not markedly change the inferred results. General distribution of  $\rho_{LD}$   
 18 and  $\rho_{AM}$  in Fig. 3 (as  $\sigma_{LD}$  and  $\sigma_{AM}$ ) also provides an overlook of both GIB1 and GIB2. Focusing on  
 19 the transects east of the sill, note that i)  $\rho_{AM}$  is generally, but not always, tilting up northward, ii)  $\rho_{LD}$   
 20 is always tilting up southward with marked GIB1-GIB2 differences close to the sill, iii) there,  $A_D$  is  
 21 relatively low during GIB1, iv)  $\rho_{LD}$  can parallel the southern slope.

1 Results (Tab. 2) first show that  $Q_L/Q$  is 40-65 % at  $4^{\circ}30'-5^{\circ}00'W$  (35-60 % for  $Q_D/Q$ ) and 70-  
2 95 % closer to the sill (5-30 % for  $Q_D/Q$ ). Assuming the transports conservation through the various  
3  $A_L$  and  $A_D$  sections, results away from the sill lead, close to the sill, to unacceptable features such as  
4 inflowing MWs. Furthermore percentages of  $\sim 50$  % are unexpected from the literature, this confirms  
5 our thoughts that the 2-layer approximation is not valid away from the sill. Results close to the sill  
6 give % values that compare well with the currently assumed LIW to WMDW ratio of 9:1, which  
7 supports our idea that LIW and WMDW have not been differentiated up to now from the whole sets  
8 of light and dense MWs. It can be noted that relying on the  $V_D$  and  $A_D$  values close to the sill leads  
9 to  $V_D$  values in the central Alboran of a few  $10^{-3} \text{ m.s}^{-1}$ , which supports our hypothesis that the dense  
10 MWs in the subbasin are quite motionless. Results show marked differences between GIB1 and  
11 GIB2 since e.g.  $Q_L/Q$  is markedly larger during GIB1 (84 to 97 %) than during GIB2 (70 to 80%),  
12 which supports our initial remark that there are no reasons to assume a constant ratio between light  
13 and dense MWs, and that this ratio can markedly change. Particularly during GIB2 when  $Q_D$  is  
14 relatively large, the interface found at more than 300 m away from the sill can be found at less than  
15 200 m near the sill ( $Z_{\min}$ , Tab.2). Also note that a relatively low  $Q_D$  east of the sill, as during GIB1  
16 vs. GIB2, is consistent with relatively low  $\sigma$  after the sill, due to the AW mixing at the sill. Finally,  
17 the maximum  $I_{LD}$  values ( $\sim 3 \cdot 10^{-2}$ ) are close to that of  $5 \cdot 10^{-2}$  inferred from Fig. 3 for the Moroccan  
18 continental slope. At the sill, dense MWs can thus easily flow along the southern slope and even  
19 over the shelf, hence possibly leading to  $\sigma$  values larger at 80 m than at 270 m.

#### 20 4.5 Another concept of the outflow

21 Describing our understanding of the outflow is simplified by considering the sea as a unique  
22 basin transforming AW into light and dense waters (LW, DW). Most of the DW formed in a shallow  
23 (2000 m) northern region reaches the bottom and amasses locally before spreading, cascading and  
24 circulating alongslope, as the whole outflow itself along the Iberian slope. The key point is that any

1 cascading of dense DW uplifts less dense DW with the major consequence that, at depths <1500 m  
2 in the Alboran subbasin in particular, the less dense uppermost DW does not circulate significantly.

3 Without any LW (in a simple idealistic case), or with DW formed in relatively large amount,  
4 the DW upper part is relatively unmixed, it easily reaches the sill depth (~300 m) and outflows there,  
5 be rotation considered or not (rotation just shifting the DW outflow northward). Such a situation was  
6 observed at the beginning of the first HCP period and we propose to consider it as an overflow (not  
7 outflow) of relatively homogeneous DW.

8 LW formed in relatively large amount amasses over DW before spreading and circulating  
9 alongslope, hence easily outflowing through the strait. A large LW amount in the strait surroundings  
10 can prevent any DW from outflowing in unmixed conditions (as during the third HCP period).

11 In general, LW and DW are formed in significant amounts during several years so that both  
12 have to outflow at Gibraltar. In the sea, AW and LW flow together counterclockwise alongslope,  
13 leading to a reduced mixing. Along its route in the northern Alboran, LW still does not strongly mix  
14 with AW, maybe because AW flows in the south so that its amount in the north is reduced (see Fig.  
15 2, 3), even though AW generally describes one or two anticyclonic gyres there (Millot, 1999). On  
16 the contrary, uplifted DW is in direct contact with AW in the south of the basin and it tends to move  
17 westward, i.e. against AW for a while. Furthermore the AW flow is very turbulent there (the  
18 Algerian Eddies), no doubts that DW in the southern Alboran is markedly mixed with AW.

19 Since LW outflows more easily than DW,  $V_L \gg V_D$  and both the small  $(\rho_D - \rho_L)$  value and  
20 rotation lead to a marked tilting up southward of  $I_{LD}$  in the strait surroundings. Assuming a constant  
21  $Q_L$ , the larger  $V_L$  the larger  $I_{LD}$  and the easier the way in which DW is brought up to the sill depth. In  
22 an extreme situation (large  $Q_L$ , large  $|I_{LD}|$ ), DW is found on the southern slope and shelf while LW is

1 found at the sill (as during the second HCP period). Whatever the case, LW and DW outflow side by  
2 side, being more juxtaposed than superposed and then easily mix individually with AW.

3 Just west of the sill, this leads to a LW and a DW juxtaposed suboutflows that are  
4 continuously stratified and that will then cascade separately alongslope. The LW suboutflow remains  
5 along the northern slope while the DW suboutflow first cascades from the southern slope towards  
6 the central part of the strait before cascading along the northern slope too. The LW and DW  
7 suboutflows are then identified as superposed LW and DW veins. The outflow characteristics  
8 downstream from the strait depend on its characteristics upstream and, more importantly, on the AW  
9 characteristics in the sill surroundings.

10

## 11 5. Conclusion

12 Considering the major differences between the current thoughts and our personal ones  
13 (section 1), we have recently undertaken a series of analyses about the Strait of Gibraltar (subsection  
14 1.2.3). We first proposed herein (section 2) a re-analysis of CTD profiles collected in 1985-1986  
15 during several campaigns (GIB1, GIB2, LYNCH-702-86) of the Gibraltar Experiment that we  
16 consider as extremely valuable and reliable. We then proposed (section 3) the analysis of two four-  
17 year CTD time series collected in 2003-2007 close to Camarinal Sill South (270 m) and on the  
18 nearby Moroccan shelf (80 m) as part of the Hydro-Changes CIESM Programme that we initiated in  
19 the early 2000s.

20 We showed that all four major MWs (WIW, LIW, TDW, WMDW) can be identified in the  
21 Alboran subbasin, hence indicating that each of the two basins of the sea produces significant  
22 amounts of both intermediate and deep waters. In the sill surroundings, we prefer considering a set

1 of light MWs (WIW, LIW, upper-TDW) and a set of dense MWs (lower-TDW, WMDW). The  
2 former circulates alongslope counterclockwise and is thus located along the northern slope. The  
3 latter is mainly uplifted and quite motionless, being possibly found just below AW along the  
4 southern slope. We also showed that any of the MWs, including LIW and WMDW, can be more or  
5 less negligible components of the outflow. The MWs outflow can mainly originate from either the  
6 eastern or the western basins, as indicated by the eastern (vs. western) dominance encountered  
7 during GIB1 (vs. GIB2) and the first (vs. second) half of the HCP experiment.

8 We identified situations (first HCP period) during which the dense MWs are relatively  
9 unmixed and flow mainly at the sill (not on the southern slope and shelf), which could be associated  
10 with what we have called an overflow. We also identified situations (third period) during which the  
11 outflow is mainly composed of light MWs. More generally, both light and dense MWs outflow  
12 together, since the western and/or the eastern basin produce, on average, both of them in significant  
13 amounts. We have shown (subsection 4.4) that a two-layer assumption and rotation can allow  
14 specifying the light vs. dense outflow characteristics just east of the sill ( $\sim 5^{\circ}15'W$  to  $5^{\circ}40'W$ ), hence  
15 supporting the GE data to demonstrate that the light-dense MWs interface can easily parallel the  
16 southern slope. Dense MWs can thus be found on the Moroccan shelf, being there eventually denser  
17 than at the sill (second HCP period). We have specified some aspects of the short-term, seasonal and  
18 long-term variabilities of the outflow characteristics (subsections 4.1, 4.2, 4.3).

19 In general, when all four MWs can be identified east of the sill, they come to be, near to the  
20 sill, less superposed than juxtaposed (the denser the more to the south) and they mix individually  
21 with AW. As demonstrated by the GIB and LYNCH data west of the sill, this leads to a series of  
22 juxtaposed suboutflows that will then cascade individually, hence regularly coming to be superposed  
23 as veins flowing northward along the Iberian slope. The outflow splitting into veins is thus due  
24 mainly to the outflow composition east of the sill, not to bathymetric features west of the sill. But the

1 veins characteristics 100-200 km from the strait depend more on the AW composition (NACW vs.  
2 SAW) and distribution in the sill surroundings than on the MWs characteristics in the sea. It is thus  
3 illusory to characterize the veins by specific hydrographic values, furthermore fortnightly and  
4 seasonal signals are created in the sill surroundings.

5 We hope that the hydrographic data analysis made herein on the basis of personal thoughts  
6 will motivate further more sophisticated studies.

7 Acknowledgements. I thank i) Frédéric Briand, general director of CIESM (Commission  
8 Internationale pour l'Exploration Scientifique de la mer Méditerranée), for his valuable and  
9 permanent support, ii) Youssef Tber for his enthusiasm in initiating the monitoring of the study area  
10 from Morocco, iii) the SHOMAR (Service Hydrographique et Océanographique de la Marine  
11 Royale du Maroc) for its efficient logistics, iv) Jean-Luc Fuda and Gilles Rougier for their help  
12 during the servicing, v) Julio Candela for providing me with his data for the tide at Tarifa, vi) Cathy  
13 and Rex Reno for their help in improving the English of a preliminary version of the paper and Paul  
14 Robertson for providing valuable comments about the writing, v) the Université de la Méditerranée  
15 and Bernard Tramier from TOTAL-ELF for their financial support, vi) AANDERAA for having  
16 lend me the currentmeter, vii) the crew of S/V *Ailes et Iles*.

## 17 References

18 Allain, C., 1964. L'hydrologie et les courants du Détroit de Gibraltar pendant l'été de 1959.  
19 Revue des Travaux de l'Institut des Pêches Maritimes, 28, 1-99.

20 Ambar, I., Howe, M.R., 1979a. Observations of the Mediterranean outflow—I. mixing in the  
21 Mediterranean outflow. Deep-Sea Research I 26A, 535–554.

- 1 Ambar, I., Howe, M.R., 1979b. Observations of the Mediterranean Outflow—II. the deep  
2 circulation in the vicinity of the Gulf of Cadiz. *Deep-Sea Research I* 26A, 555–568.
- 3 Ambar, I., 1983. A shallow core of Mediterranean Water off Western Portugal. *Deep-Sea*  
4 *Research I* 30, 677–680.
- 5 Ambar, I., Armi, L., Bower, A., Ferreira, T., 1999. Some aspects of time variability of the  
6 Mediterranean Water off South Portugal. *Deep-Sea Research I* 46, 1109–1136.
- 7 Ambar, I., Serra, N., Brogueira, M.J., Cabeçadas, G., Abrantes, F., Freitas, P., Gonçalves, C.,  
8 Gonzales, N., 2002. Physical, chemical and sedimentological aspects of the Mediterranean outflow  
9 off Iberia. *Deep-Sea Research II* 49, 4163-4177.
- 10 Baringer, M., Price, J., 1997. Mixing and spreading of the Mediterranean outflow. *Journal of*  
11 *Physical Oceanography* 27, 16 54-1677.
- 12 Baringer, M., Price, J., 1999. A review of the physical oceanography of the Mediterranean  
13 outflow. *Marine Geology*, 155, 63-82.
- 14 Béthoux, J.P., Gentili, B., Raunet, J., Tailliez, D., 1990. Warming trend in the Western  
15 Mediterranean Deep Water. *Nature*, 347, 660-662.
- 16 Borenäs, K.M., Wahlin, A.K., Ambar, I., Serra, N., 2002. The Mediterranean outflow  
17 splitting – a comparison between theoretical models and Canigo data. *Deep-Sea Research, II* 49,  
18 4195-4205.
- 19 Bray, N.A., Ochoa, J., Kinder, T.H., 1995. The role of the interface in exchange through the  
20 Strait of Gibraltar. *Journal of Geophysical Research*, 100, C6, 10755-10776.

- 1           Bryden, H.L., Millard, R.C., Porter, D.L., 1978. CTD observations in the western  
2   Mediterranean sea during cruise 118, Leg 2 of R/V Chain, February 1975. Woodw Hole  
3   Oceanographic Institution Technical Report, 78-26, March, 38pp.
- 4           Bryden, H.L., Stommel, H.M., 1982. Origin of the Mediterranean outflow. *Journal of Marine*  
5   *Research*, 40, (Suppl.), 55-71.
- 6           Bryden, H.L., Stommel, H.M., 1984. Limiting processes that determine basic features of the  
7   circulation in the Mediterranean Sea. *Oceanol. Acta* 7, 289–296.
- 8           Bryden, H.L., Kinder, T.H., 1991. Recent progress in strait dynamics. *Reviews of*  
9   *Geophysics*, (Supp.), 617-631.
- 10          Bryden, H.L., Candela, J., Kinder, T.H., 1994. Exchange through the Strait of Gibraltar.  
11   *Progress in Oceanography*, 33, 201-248.
- 12          Candela, J., Winant, C., Ruiz, A., 1990. Tides in the Strait of Gibraltar. *Journal of*  
13   *Geophysical Research*, 95(C5), 7313--7335.
- 14          Davies, P.A., Guo, Y., Rotenberg, E., 2002. Laboratory model studies of Mediterranean  
15   outflow adjustment in the Gulf fo Cadiz. *Deep-Sea Research II*, 49, 4207-4223.
- 16          Gascard, J.C., Richez, C., 1985. Water masses and circulation in the western Alboran Sea and  
17   in the Straits of Gibraltar. *Progress in Oceanography*, 15, 157-216.
- 18          Howe, M., Abdullah, M., Deetae, S., 1974. An interpretation of the double T-S maxima in  
19   the Mediterranean outflow using chemical tracers. *Journal of Marine Research*, 32 (3), 377-386.
- 20          Johnson, J., Ambar, I., Serra, N., Stevens, I., 2002. Comparative studies of the spreading of  
21   Mediterranean water through the Gulf of Cadiz. *Deep-Sea Research II*, 49, 4179-4193.

1           Kinder, T.H., Parrilla, G., 1987. Yes, some of the Mediterranean outflow does come from  
2           great depths. *Journal of Geophysical Research*, 92, C3, 2901-2906.

3           Lacombe, H., Richez, C., 1982. The regime of the Straits of Gibraltar. In: *Hydrodynamics of*  
4           *semi-enclosed seas*, J.C.J. Nihoul, editor, Elsevier, Amsterdam, 13-74.

5           Madelain, F., 1970. Influence de la topographie du fond sur l'écoulement Méditerranéen  
6           entre le Détroit de Gibraltar et le Cap Saint-Vincent. *Cahiers Océanographiques* 22, 43–61.

7           MEDAR Group, 2002. MEDATLAS/2002 database. Mediterranean and Black Sea database  
8           of temperature salinity and bio-chemical parameters. Climatological Atlas. IFREMER Edition (4  
9           CDroms).

10          Millot, C., 1999. Circulation in the Western Mediterranean sea. *J. March Systems*, 20, 1-4,  
11          423-442.

12          Millot, C., 2007. Interannual salinification of the Mediterranean inflow. *Geophysical Research*  
13          *Letters*, 34, L21069, doi:10.1029/2007/GL031179. [www.ifremer.fr/lobtln](http://www.ifremer.fr/lobtln)

14          Millot, C., 2008. Short-term variability of the Mediterranean in- and out-flows. *Geophysical*  
15          *Research Letters*, 35, L15603, doi:10.1029/2008/GL033762. [www.ifremer.fr/lobtln](http://www.ifremer.fr/lobtln)

16          Millot, C., and I. Taupier-Letage (2005a), Circulation in the Mediterranean Sea, in *The*  
17          *Handbook of Environmental Chemistry, Vol.5: Water Pollution*, Part K, pp. 29-66, Springer-Verlag,  
18          Berlin-Heidelberg, doi: 10.1007/b107143. <http://dx.doi.org/10.1007/b107143>, [www.ifremer.fr/lobtln](http://www.ifremer.fr/lobtln)

19          Millot C. and I. Taupier-Letage, 2005b. Additional evidence of LIW entrainment across the  
20          Algerian Basin by mesoscale eddies and not by a permanent westward-flowing vein. *Progress in*  
21          *Oceanography*, 66, 231-250. [www.ifremer.fr/lobtln](http://www.ifremer.fr/lobtln)

- 1 Millot C., J. Candela, J.-L. Fuda and Y. Tber, 2006. Large warming and salinification of the  
2 Mediterranean outflow due to changes in its composition. *Deep-Sea Res.*, 53/4, 656-666.  
3 doi:10.1016/j.dsr.2005.12.017. [www.ifremer.fr/lobtln](http://www.ifremer.fr/lobtln)
- 4 Ochoa, J., Bray, N.A., 1991. Water mass exchange in the Gulf of Cadix. *Deep-Sea Research*,  
5 38, (Suppl. 1), 465-503.
- 6 Parrilla, G., Kinder, T.H., Bray, N.A., 1989. Hidrologia del Agua Mediterranea en el  
7 Estrecho de Gibraltar durante el Experimento Gibraltar (Octubre, 1985 – Octubre, 1986). In  
8 Seminario sobre la oceanografia fisica del Estrecho de Gibraltar, Madrid 24-28 Octubre, 1988,  
9 edited by J.L. Almazan, H. Bryden, T. Kinder and G. Parrilla, 95-121.
- 10 Pettigrew, N.R., 1989. Direct measurements of the flow of Western Mediterranean Deep  
11 Water over the Gibraltar sill. *Journal of Geophysical Research*, 94, C12, 18089-18093.
- 12 Roether, W., Manca, B., Klein, B., Bregant, D., Georgopoulos, D., Beitzl V., Kova, V.,  
13 Luchetta, A., 1996. Recent changes in Eastern Mediterranean Deep Waters. *Science*, 271, 333-335.
- 14 Sannino, G., Bargagli, A., Artale, V., 2002. Numerical modeling of the mean exchange  
15 through the Strait of Gibraltar. *Journal of Geophysical Research*, 107, C8, 3094,  
16 doi:10.1029/2001JC000929.
- 17 Serra, N., Ambar, I., 2002. Eddy generation in the Mediterranean Undercurrent. *Deep-Sea*  
18 *Research II* 49 (19), 4225–4243.
- 19 Siedler, G., 1968. The frequency distribution of water types in the outflow region of straits.  
20 *Kieler Meeresforschung* 24, 59-65.

- 1            Sparnocchia, S., Gasparini, G.P., Astraldi, M., Borghini, M., Pistek, P., 1999. Dynamics and  
2 mixing of the Eastern Mediterranean Outflow in the Tyrrhenian Basin. *J. March Sys.* 20, 301–317.
- 3            Vargas-Yanez, M., Ramirez, T., Cortes, D., Sebastian, M., 2002. Warming trends in the  
4 continental shelf of Malaga Bay (Alboran Sea). *Geophysical Research Letters*, 29, 22, 2082,  
5 doi:10.1029/2002GL015306.
- 6            Vargas, J. M., García-Lafuente, J., Candela, J., Sánchez, A.J., 2006. Fortnightly and monthly  
7 variability of the exchange through the Strait of Gibraltar. *Progress in Oceanography*,  
8 doi:10.1016/j.pocean.2006.07.001.
- 9            Wesson, J.C., Gregg, M.C., 1994. Mixing at Camarinal Sill in the Strait of Gibraltar. *Journal of*  
10 *Geophysical Research*, 99, C3, 9847-9878.
- 11           Wu, W., Danabasoglu, G., Large, W.G., 2007. On the effects of parameterized Mediterranean  
12 overflow on North Atlantic ocean circulation and climate. *Ocean Modelling*, 19 (1-2), 31-52.
- 13           Zenk, W., 1975. On the origin of the intermediate double maxima in T/S profiles from the  
14 North Atlantic. *Meteor Forschungsergebnisse A* 16, 35–43.

15

16            Figure Captions.

17            Figure 1. The study area with the schematized GE transects (in blue) together with the HPC  
18 270-m site (red dot, 35°55.2'N-5°45.0'W, on a small plateau ~1.1 km north of the ~300-m deepest  
19 part of Camarinal Sill South (CSS, green dashed line)), and the 80-m one (orange dot, 35°52.8'N-  
20 5°43.5'W) that are at ~10 and 5 km from the Moroccan coast.

1           Figure 2. Schematic diagram of the circulation of AW and all major MWs together with the  
2 major subbasins, islands and channels in the western basin of the Mediterranean Sea. All waters  
3 mainly flowing counterclockwise alongslope are represented by full lines in an on-offshore direction  
4 as seen from above. Dashed lines represent i) for AW its seaward spreading due to the mesoscale  
5 Algerian Eddies, ii) for LIW and TDW their entrainment away from the Sardinian slope by these  
6 eddies, iii) for WIW and WMDW in the north of the basin their zone of formation, iv) for WMDW  
7 in the Alboran its uplifting and relatively low circulation. More details are given in the text, as well  
8 as in Millot (1999) and Millot and Taupier-Letage (2005a).

9           Figure 3. North-south bathymetric sections inferred from a navigation chart with a 5 nm  
10 interval aimed at comparing the transects areas, hence plotted with similar y-latitude (in tens of  
11 degrees) and z-depth (in km) scales. Specific bathymetric features, such as Camarinal Sill centered at  
12  $\sim 5^{\circ}45'W$  but orientated NNW-SSE, are roughly represented, and some transects are not exactly  
13 north-south or straight. Isopycnals  $\sigma_{LD}=29.08 \text{ kg.m}^{-3}$  and  $\sigma_{AM}=28.75 \text{ kg.m}^{-3}$  are in blue and red,  
14 respectively, for GIB1 (full) and GIB2 (dashed) east of the sill; west of it,  $\sigma_{AM}=27.0 \text{ kg.m}^{-3}$  (violet)  
15 while  $\sigma_{LD}=29.0, 28.5$  and  $28.0 \text{ kg.m}^{-3}$  (cyan) at  $5^{\circ}50'W, 6^{\circ}05'W$  and  $6^{\circ}15'W$ , respectively. Isopycnal  
16 coloring is reproduced in sections thereafter. The red and orange dots ( $5^{\circ}45'W$ ) represent the CTD  
17 sites at 270 and 80 m.

18           Figure 4.  $\theta$ -S diagrams for the  $4^{\circ}30'W$  transect: GIB1 (a), GIB2 (b), both (c). Till  $5^{\circ}50'W$ , the  
19  $\theta$  and S scales are the same and arbitrarily fixed acronyms (see text) are still at the same place. In  
20 both a) and b), the red profiles indicate the WIW and/or LIW cores, the violet profiles indicate  
21 marked influence of the WIW and/or LIW veins while the blue profiles indicate a direct mixing  
22 between AW and either lower-TDW or WMDW (no influence of either WIW or LIW). In c), the

1 GIB1 (respectively GIB2) profiles are orange (respectively brown). Isopycnals are plotted 0.05  
2  $\text{kg.m}^{-3}$  apart.

3 Figure 5. The 4°30'W GIB1 and GIB2 transects in salinity (S1 and S2), potential temperature  
4 (T1 and T2) and potential density anomaly (D1 and D2). Profiles are colored as explained in Fig. 4  
5 and indicated in Tab. 1. For S1 and S2,  $S=38.00$  is thick,  $S=38.45$  is dashed,  $S>38.435$  are in grey.  
6 For T1 and T2,  $\theta=13.05$  °C is thick,  $\theta=12.825$  °C and  $\theta=13.00$  °C are dashed,  $\theta<12.90$  °C are in  
7 grey. For D1 and D2,  $\sigma=28.75$   $\text{kg.m}^{-3}$  is red,  $\sigma=29.08$   $\text{kg.m}^{-3}$  is blue (as in Fig. 3),  $\sigma=29.05$   $\text{kg.m}^{-3}$   
8 and  $\sigma=29.09$   $\text{kg.m}^{-3}$  are dashed (see subsection 4.4) and  $\sigma>29.085$   $\text{kg.m}^{-3}$  are in grey. Most profiles  
9 were down to (thin line and light grey area) a few metres above the bottom (thick line and dark grey  
10 area); in general, the maximum-depth and bottom-depth lines cannot be differentiated on the figures.  
11 The northern and southern limits of the transect (depth =0) are not realistic (see Fig. 3) and were  
12 arbitrarily fixed not too far the nearest profile, but information there is not reliable. Most of these  
13 values and comments apply till 6°15'W.

14 Figure 6. As in Fig. 4 for 5°00'W.

15 Figure 7. As in Fig. 5 for 5°00'W.

16 Figure 8. As in Fig. 4 for 5°15'W.

17 Figure 9. As in Fig. 5 for 5°15'W.

18 Figure 10. As in Fig. 4 for 5°30'W.

19 Figure 11. As in Fig. 5 for 5°30'W.

20 Figure 12. As in Fig. 4 for 5°40'W.

1 Figure 13. As in Fig. 5 for 5°40'W.

2 Figure 14.  $\theta$ -S diagrams at 5°50'W for GIB1 (a), GIB2 (b) and LYNCH (c) with scales as in  
3 Fig. 4 (MWs acronyms are no more informative). Profiles numbers (GIB locations in Fig. 17) from  
4 south to north are specified at the largest  $\sigma$  value. Colors for a) and b) are as before (see Fig. 4).  
5 Color for c) is green for transects 1,2 at the beginning (#2 only once) and cyan for transects 3,4 at the  
6 end (~10 days after, #1 only once).

7 Figure 15.  $\theta$ -S diagrams at 5°50'W (a, all plots in Fig. 14) and 6°05'W (b, all plots in Fig. 18)  
8 in reduced ranges to focus on the  $\sigma_{\max}$  values specified by dots that are pink (WIW), red (LIW),  
9 violet (TDW), blue (WMDW), grey (unspecified, LYNCH)) for GIB1 (orange), GIB2 (brown),  
10 LYNCH12 (green) and LYNCH34 (cyan).

11 Figure 16A. Same as in Fig. 14 but for MWs wider ranges (same till 6°15'W). Additional  
12 profiles in the northern part of the GIB1 and GIB2 transects were out of range in Fig. 14. To better  
13 differentiate the profiles, dots are replaced by the profile #. Isopycnals are 0.1 kg.m<sup>-3</sup> apart. Profiles  
14 #2/LYNCH12 and #1/LYNCH34 were performed only once.

15 Figure 16B. Same as in Fig. 16A but for wider ranges to represent both the MWs and AW  
16 (NACW and SAW; see definitions in the text). Isopycnals are 1.0 kg.m<sup>-3</sup> apart.

17 Figure 17. Same as in Fig. 5 for 5°50'W.  $\sigma=27.0$  kg.m<sup>-3</sup> is violet and  $\sigma=29.0$  kg.m<sup>-3</sup> is cyan.

18 Figure 18. Same as in Fig. 16A for 6°05'W.

19 Figure 19. As in Fig. 5 for 6°05'W. Densities  $> \sigma = 28.5$  kg.m<sup>-3</sup> (cyan) are in grey,  $\sigma = 28.75$   
20 kg.m<sup>-3</sup> is thick,  $\sigma=27.0$  kg.m<sup>-3</sup> is violet.

1           Figure 20. As in Fig. 5 for 6°15'W and specific isolines.  $S = 36.0$  (dashed) emphasizes the  
2    AW  $S_{\min}$ ,  $S = 37.0$  (thick) represents the AW-MWs interface,  $S > 37.5$  (grey) represents unmixed  
3    MWs, the largest isoline value is  $S = 38.0$ . In T1 and T2,  $\theta < 13.0$  °C (dashed) are in lattice grey,  $\theta$   
4     $= 13.185$  °C (thick) locates the vein on the bottom at #6/GIB2. In D1 and D2,  $\sigma = 27.0$   $\text{kg.m}^{-3}$  (violet)  
5    represents the AW-MWs interface,  $\sigma > 28.0$   $\text{kg.m}^{-3}$  (cyan) are in grey, the largest isoline value is  $\sigma$   
6     $= 28.5$   $\text{kg.m}^{-3}$ .

7           Figure 21.  $\theta$ - $S$  diagrams at 6°15'W for GIB1 (a), GIB2 (b) and both(c) showing WIW (pink),  
8    LIW (red), TDW (violet) and WMDW (blue). Isopycnals are 0.1  $\text{kg.m}^{-3}$  apart.

9           Figure 22.  $\theta$ - $S$  diagrams from the 2003-2007 (Julian days #12 to #1536) time series at 270  
10   and 80 m and the six periods (a to f) specified in the text. The whole time series are plotted with light  
11   grey dots (270 m) and dark grey ones (80 m), together with  $\sigma = 29.05$  and  $29.10$   $\text{kg.m}^{-3}$ . The colors  
12   significance and the date intervals for each of the periods are specified in both the text and the  
13   figure. Dashed lines connect consecutive data and provide information about mixing.

14          Figure 23. Density ( $\sigma$ ) data measured (grey dots) and selected with the sd criterion (cyan  
15   dots) for the MWs at 270 m from January 12 to July 27, 2003, together with the daily moving  
16   averages of the measured density (blue curve) and speed ( $V$ ) toward 225 °T (black curve); tidal  
17   amplitude at Tarifa (maxima  $\sim 80$  cm) is from Julio Candela (personal communication).

18          Figure 24. Polynomial (degree 3) fits from the  $S$  (a),  $\theta$  (b), and  $\sigma$  (c) data at 270 m during  
19   year #1 (full line), #2 (large dashed line), #3 (small dashed line) and #4 (dashed dotted line). Black  
20   lines correspond to the whole set of data measured in the MWs displayed ranges. Red lines  
21   correspond to regularly distributed data selected with a tidal criterion ( $S_{\max}$ ,  $\theta_{\min}$  and  $\sigma_{\max}$  over 12-h

1 successive intervals) while blue lines correspond to the same amount of data selected with the sd  
2 criterion (hence irregularly distributed).

3 Figure 25. Monthly moving averages of the number of S (blue),  $\theta$  (red) and  $\sigma$  (green) data  
4 selected with the sd criterion (30 %) for AW at 80 m (a), the MWs at 80 m (b) and the MWs at 270  
5 m (c); corresponding triplets are in black. The more homogeneous AW is encountered in the second  
6 half of February (dashed lines). See text and Millot (2007) for details.

7 Table 1. Beginning time of the GIB1 and GIB2 CTD profiles. Also specified are the dates of  
8 the first and last profiles for each transect, as well as the profile color (see text).

9 Table 2. The slope of the light-dense MWs interface  $I_{LD}$  for the GIB1 and GIB2 transects east  
10 of the sill is inferred from a linear fit of  $\sigma = 29.08 \text{ kg.m}^{-3}$ ; specified characteristics are its minimum  
11 immersion ( $Z_{\min}$ ), vertical range ( $\Delta Z$ ), width ( $Y$ ) and numerical value. The  $A_L$  and  $A_D$  sections areas  
12 are inferred from bathymetric profiles (Fig. 3) and from a AW-MWs interface identified with  $\sigma$   
13  $= 28.75 \text{ kg.m}^{-3}$ .  $V_L$ ,  $V_D$ ,  $Q_L$  and  $Q_D$  are computed as specified in the text.

14

15

Figure 1  
[Click here to download high resolution image](#)

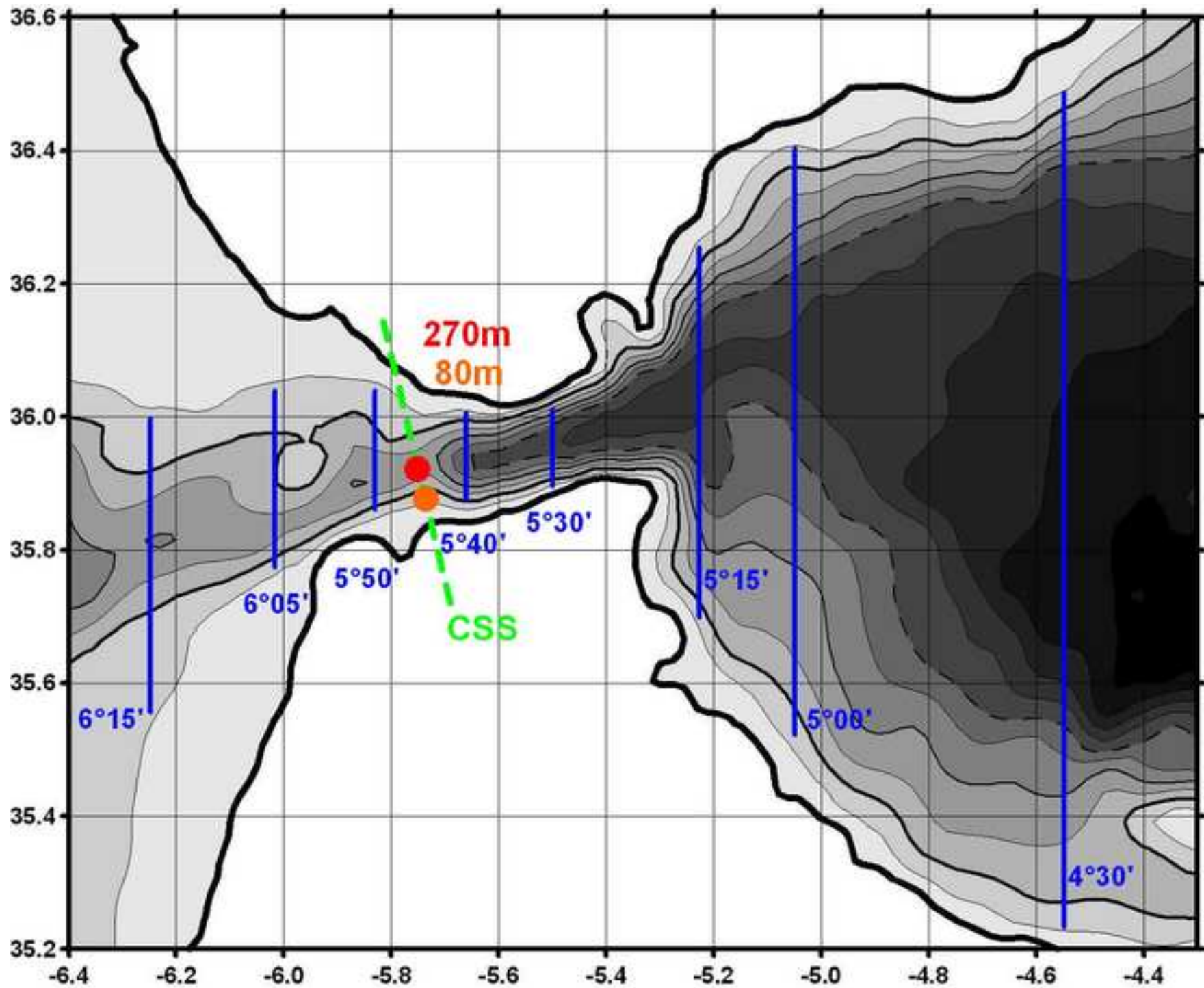


Figure 2  
[Click here to download high resolution image](#)

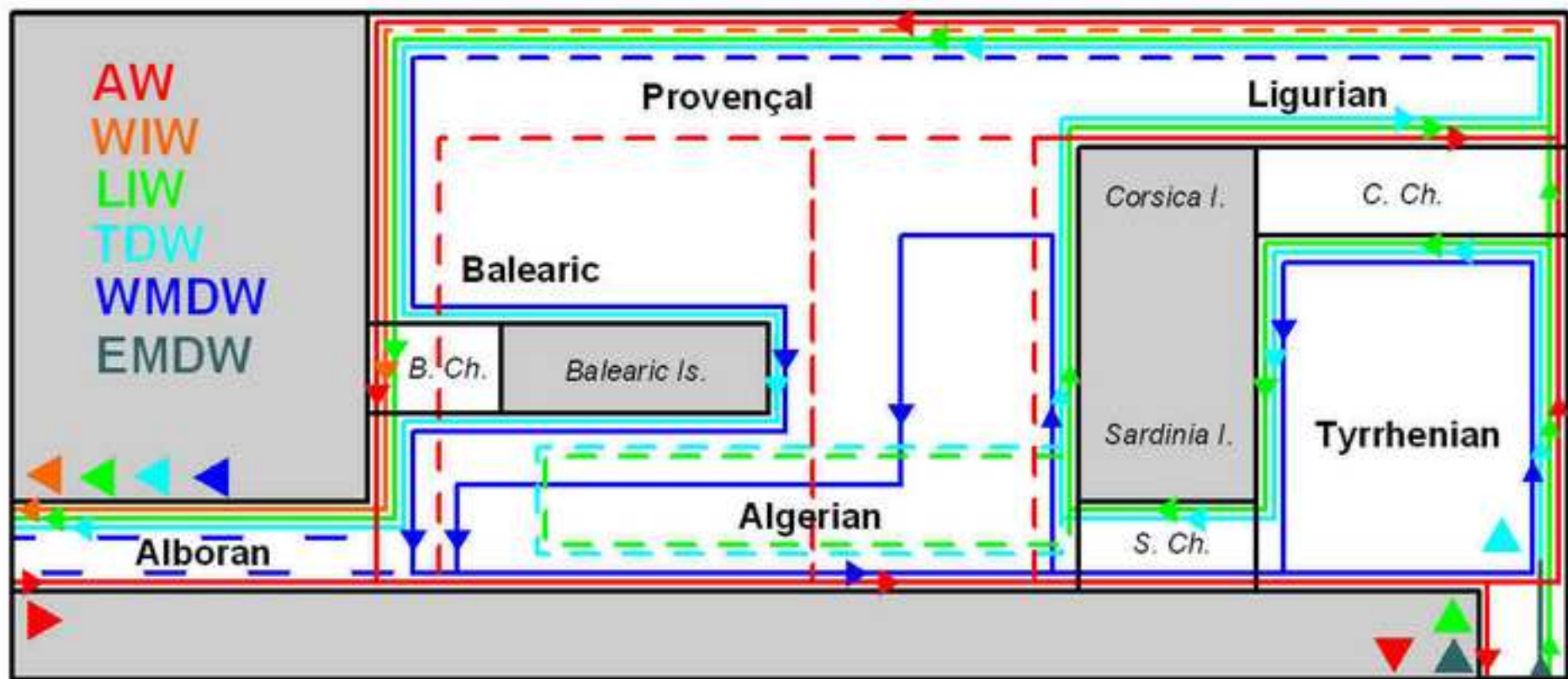


Figure 3  
[Click here to download high resolution image](#)

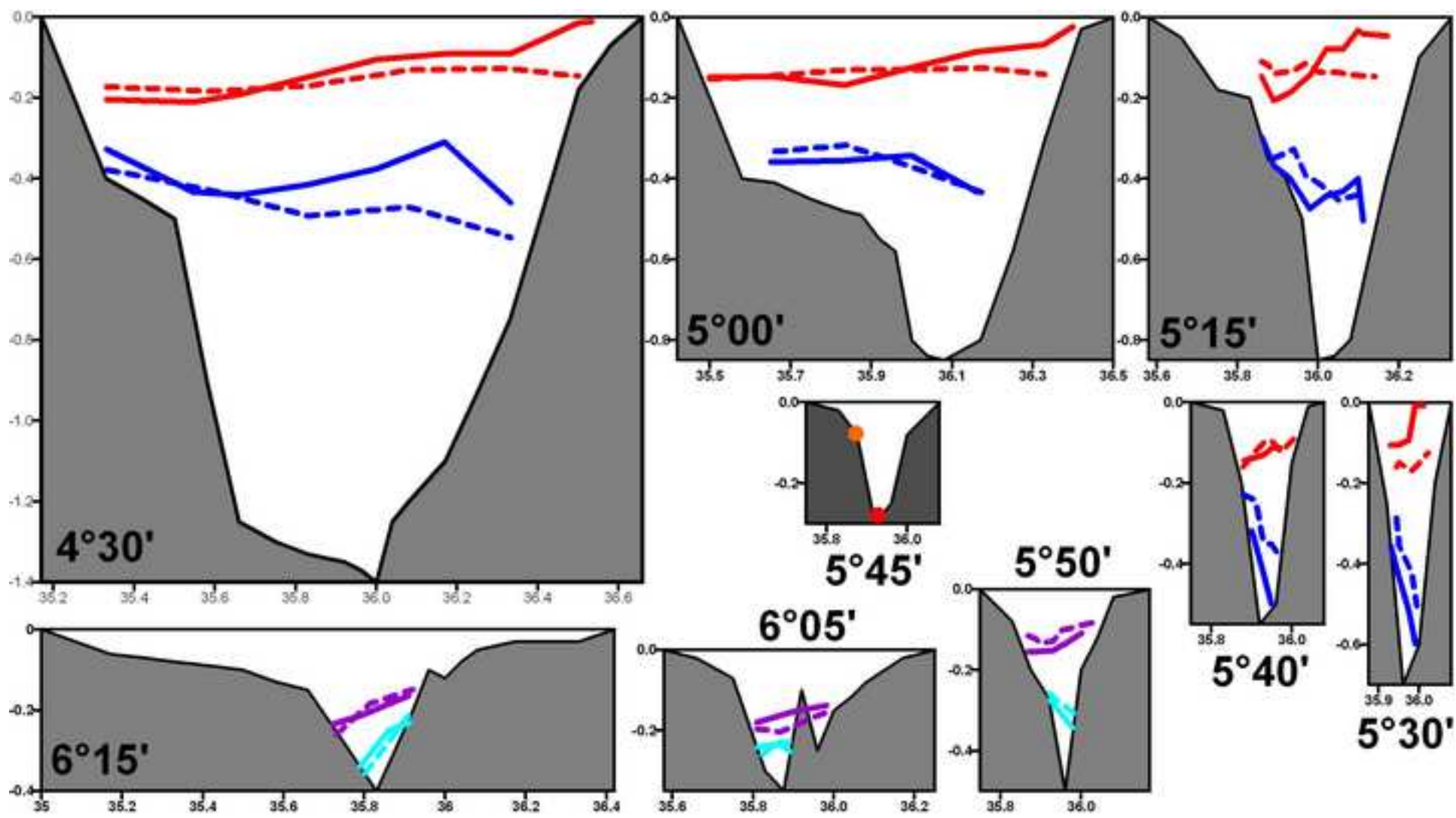


Figure 4  
[Click here to download high resolution image](#)

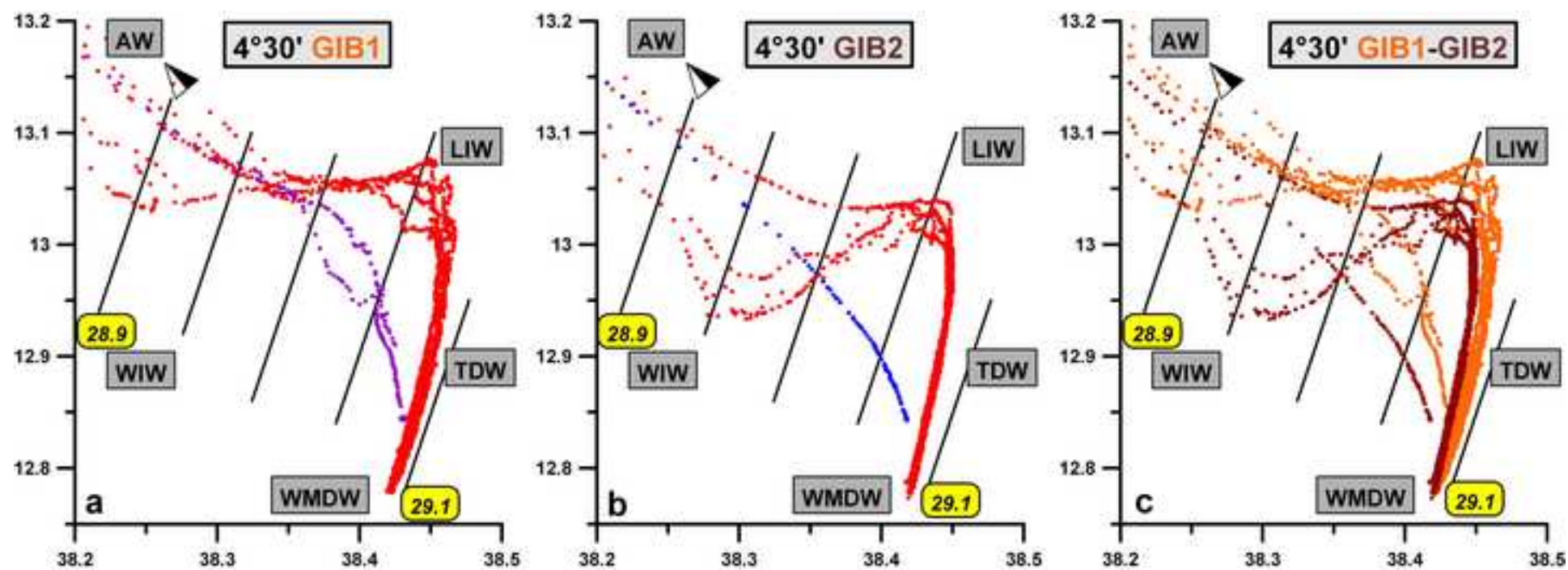


Figure 5  
[Click here to download high resolution image](#)

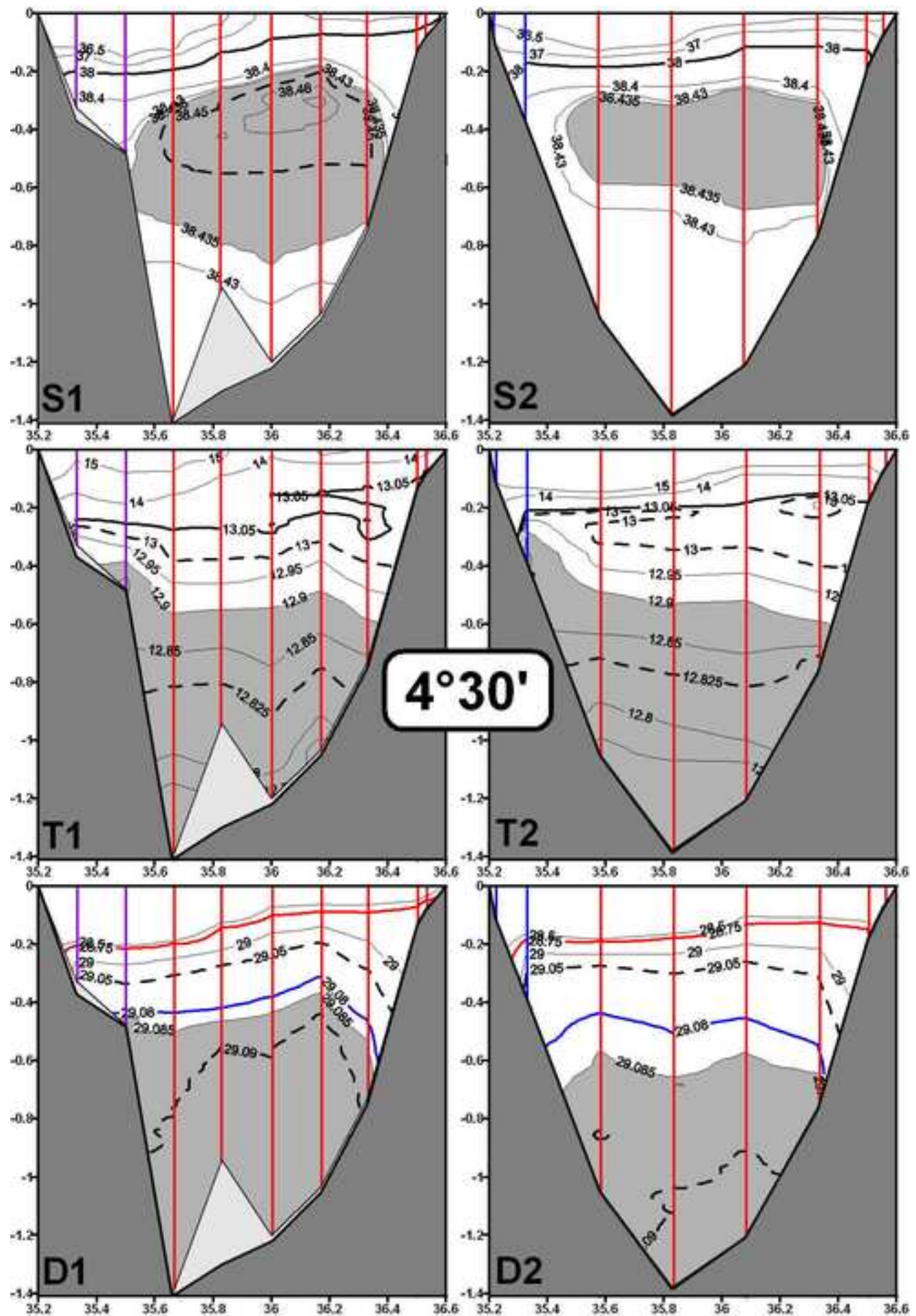


Figure 6  
[Click here to download high resolution image](#)

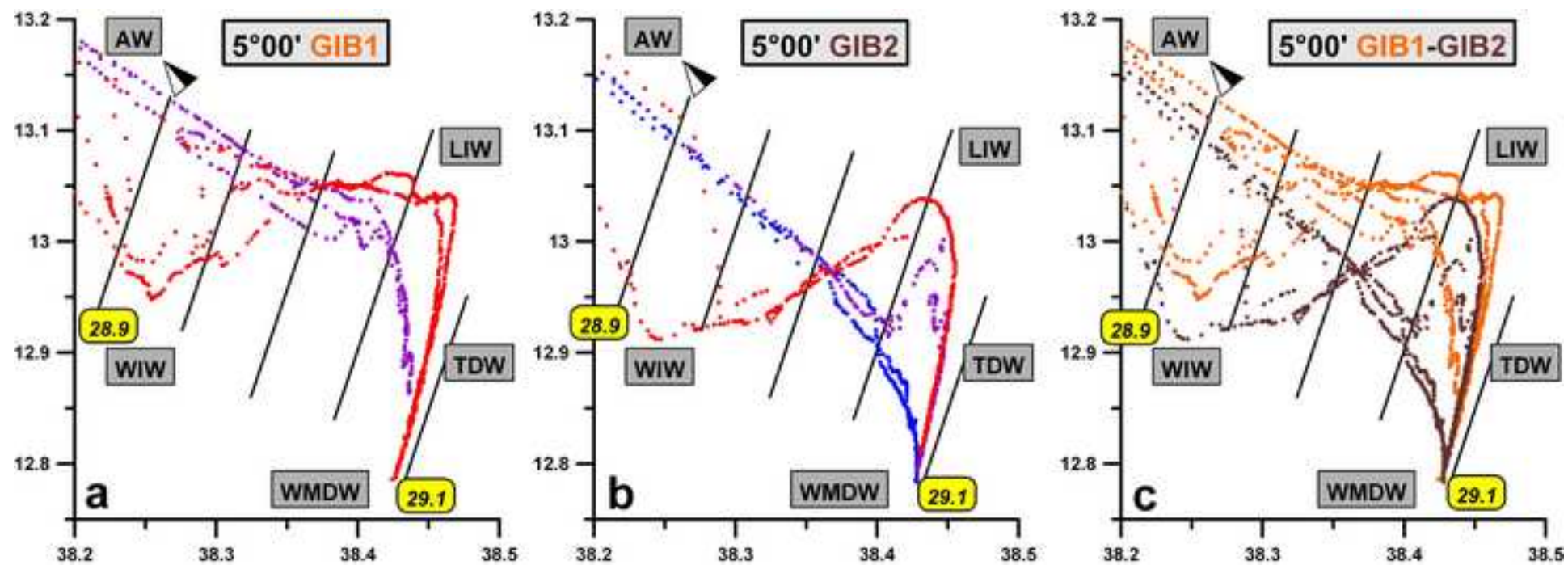


Figure 7  
[Click here to download high resolution image](#)

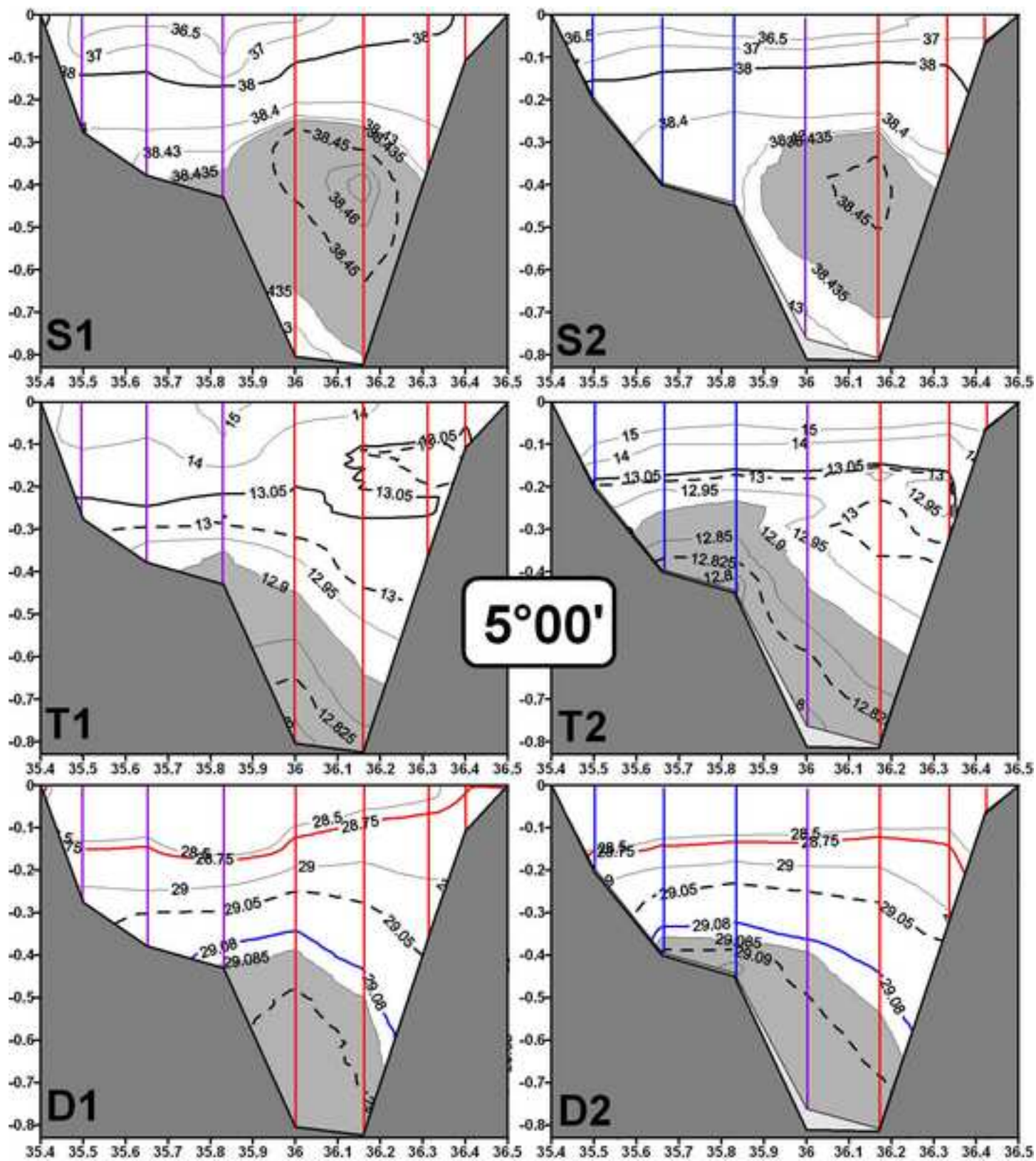


Figure 8  
[Click here to download high resolution image](#)

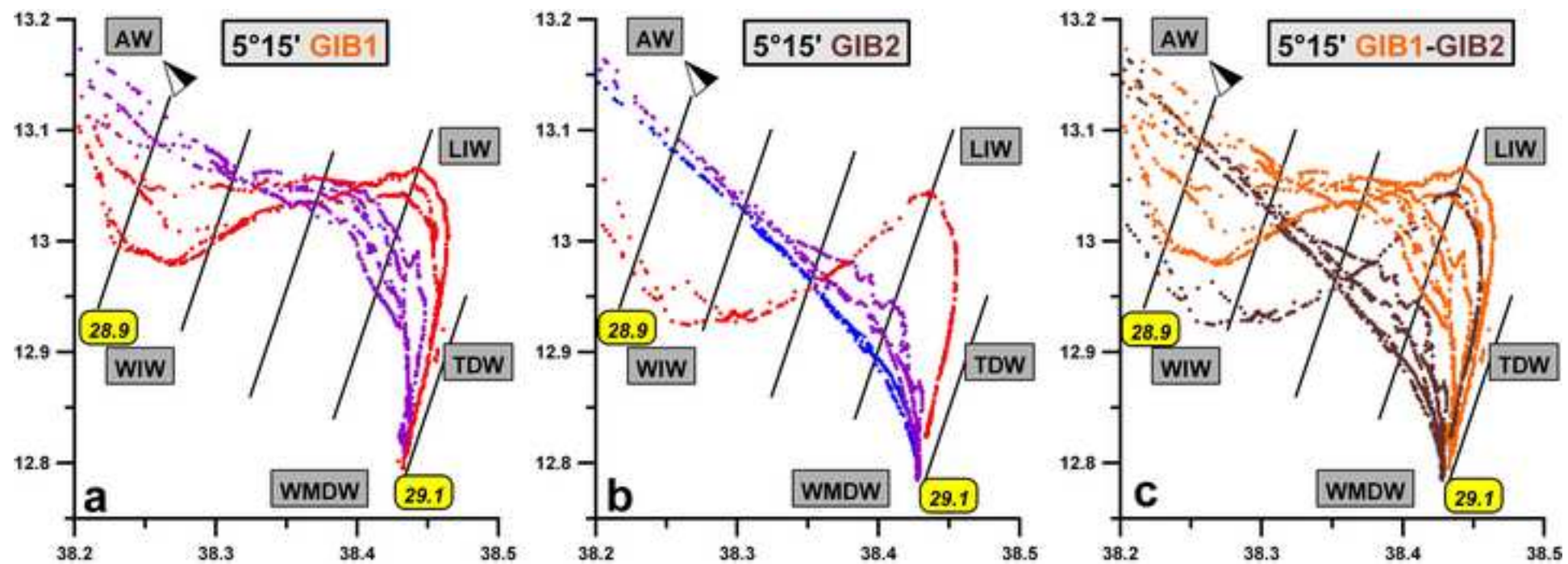


Figure 9  
[Click here to download high resolution image](#)

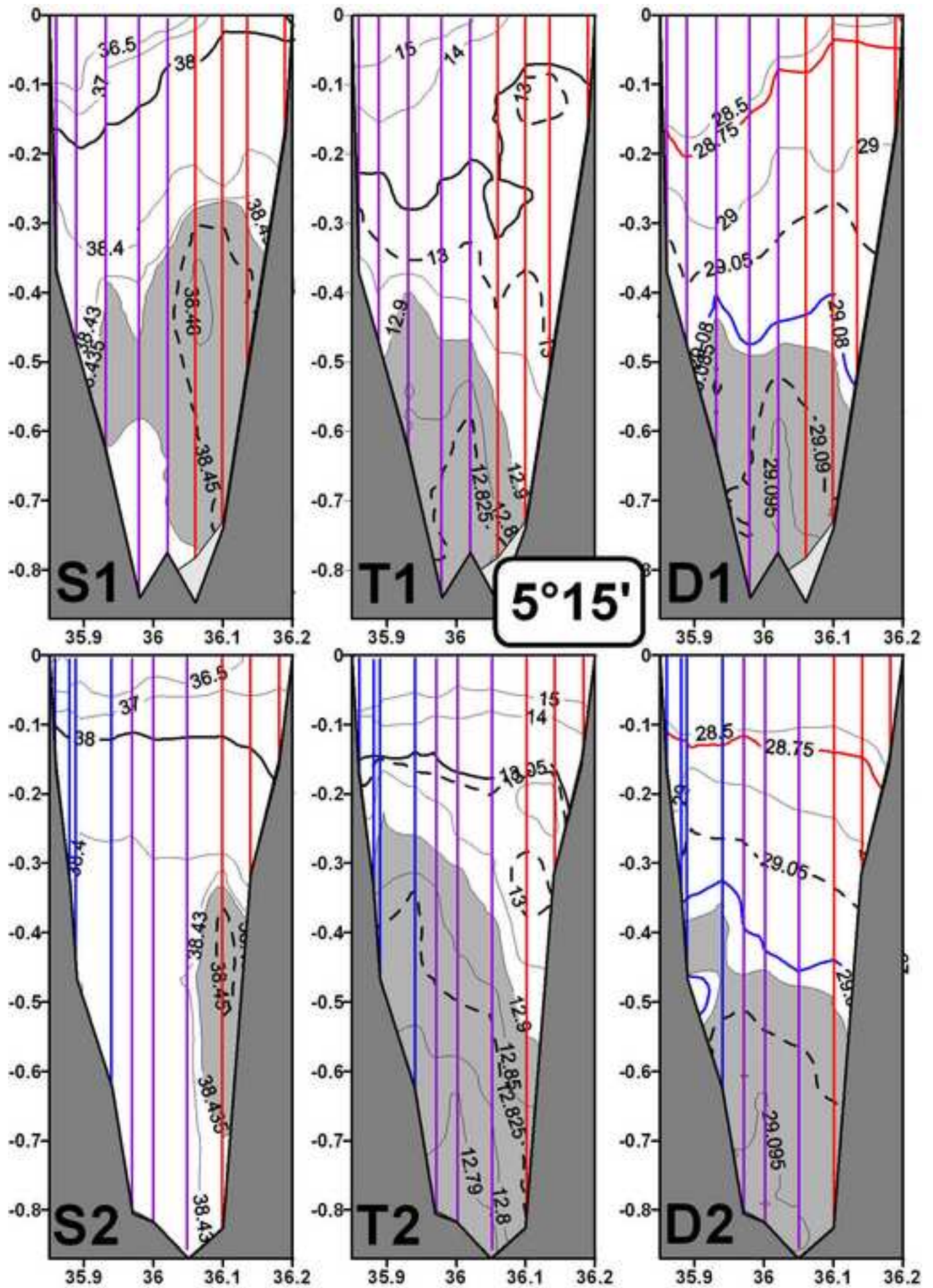


Figure 10  
[Click here to download high resolution image](#)

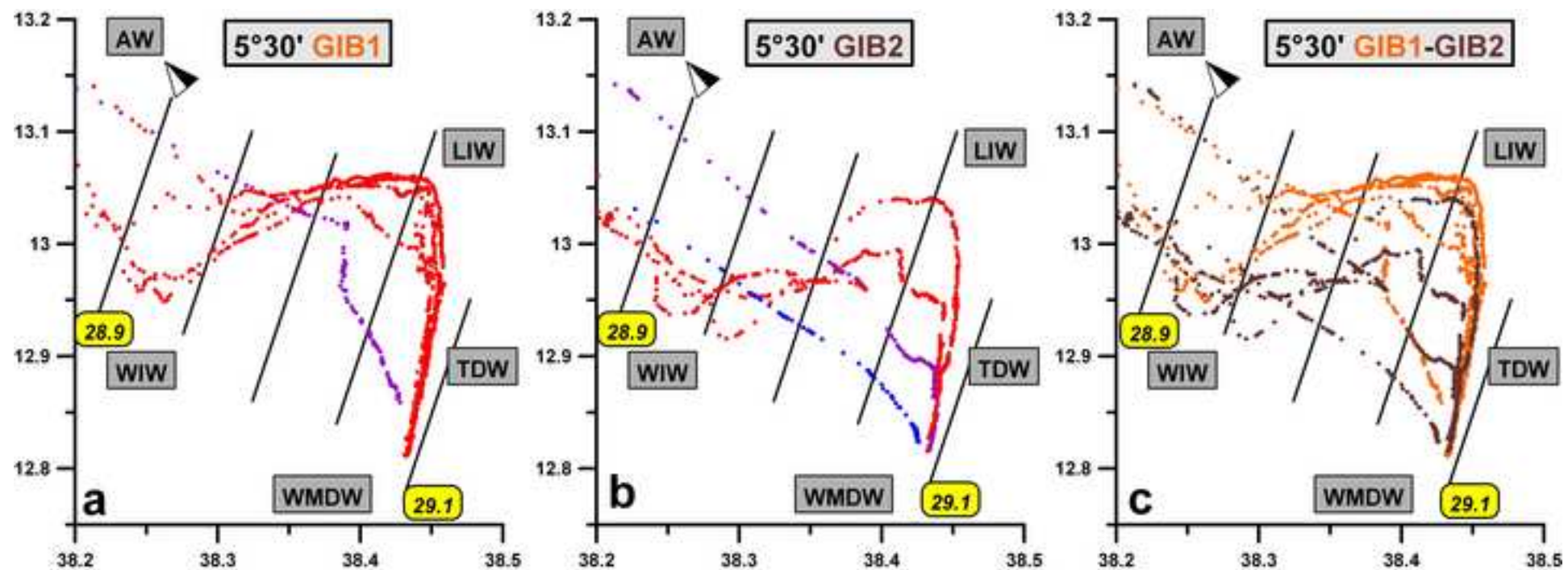


Figure 11  
[Click here to download high resolution image](#)

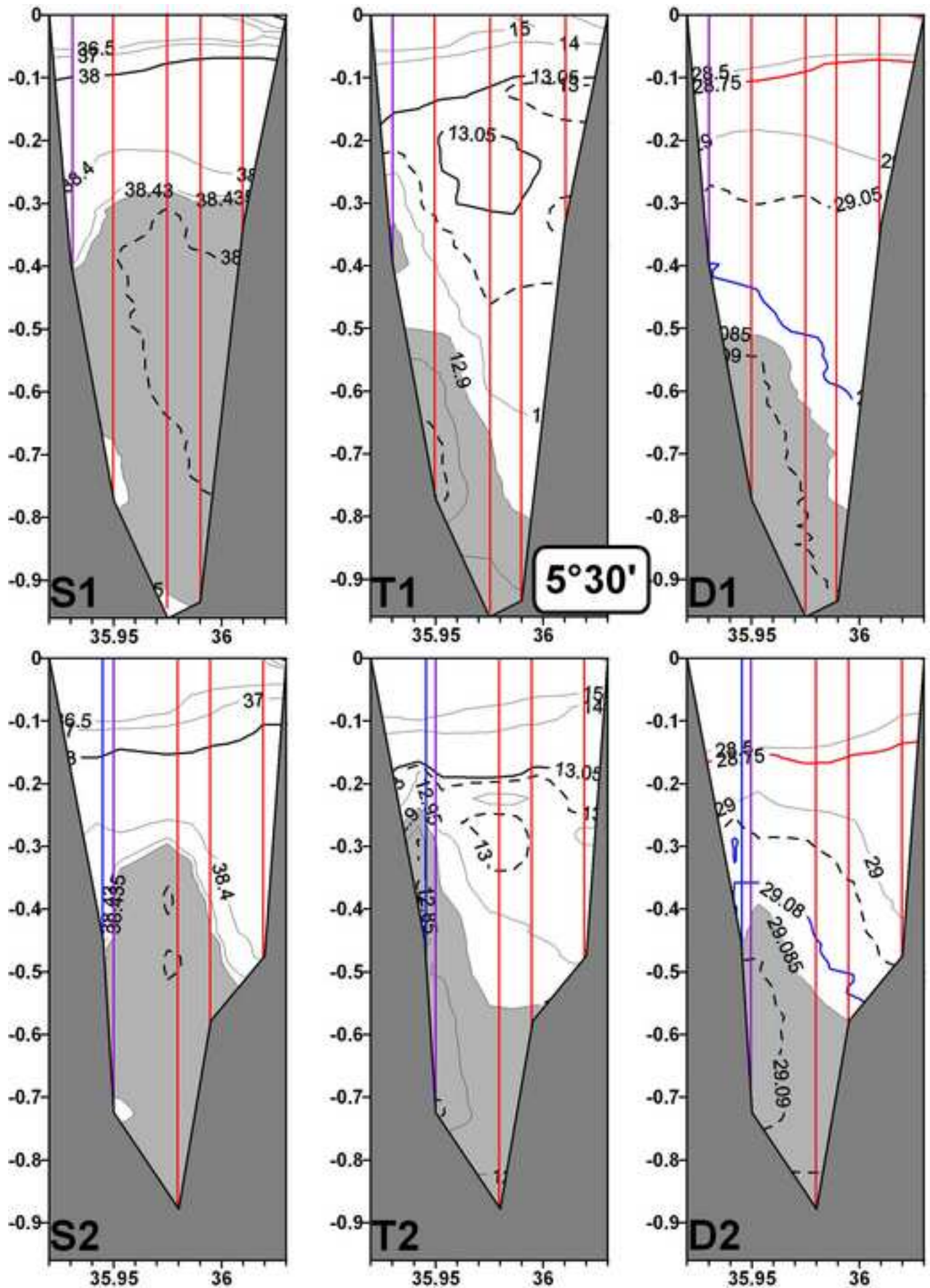


Figure 12  
[Click here to download high resolution image](#)

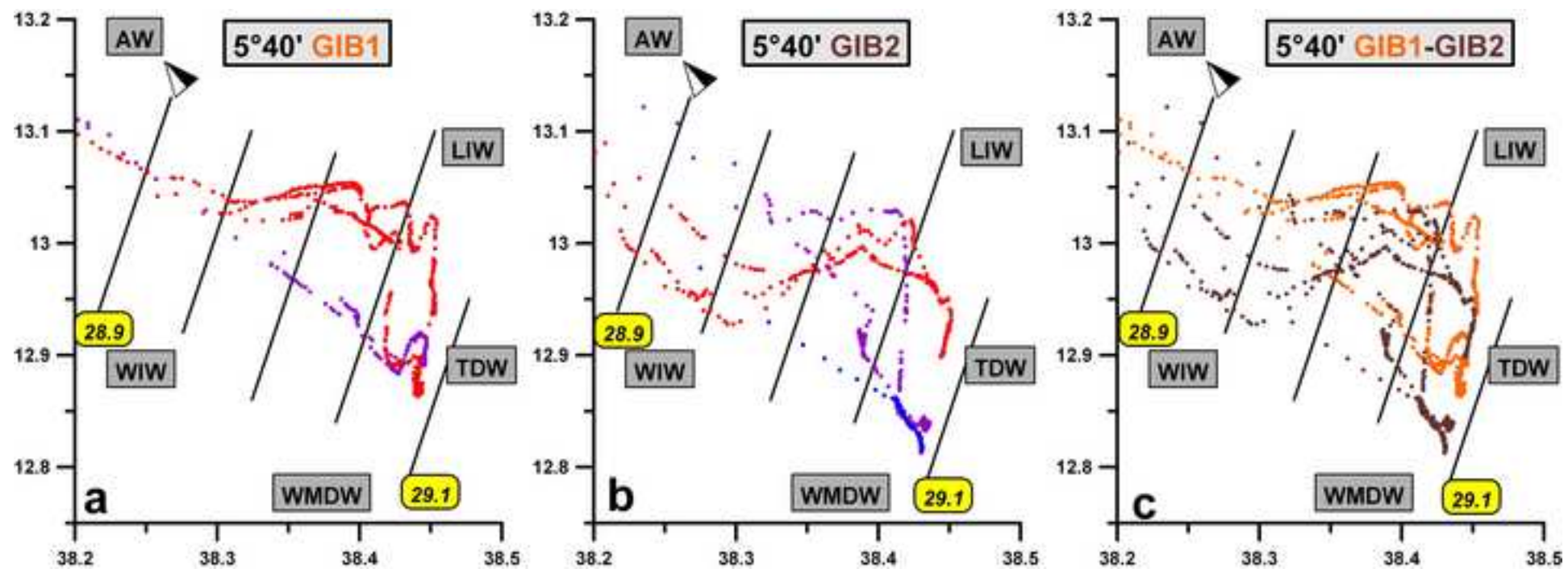


Figure 13

[Click here to download high resolution image](#)

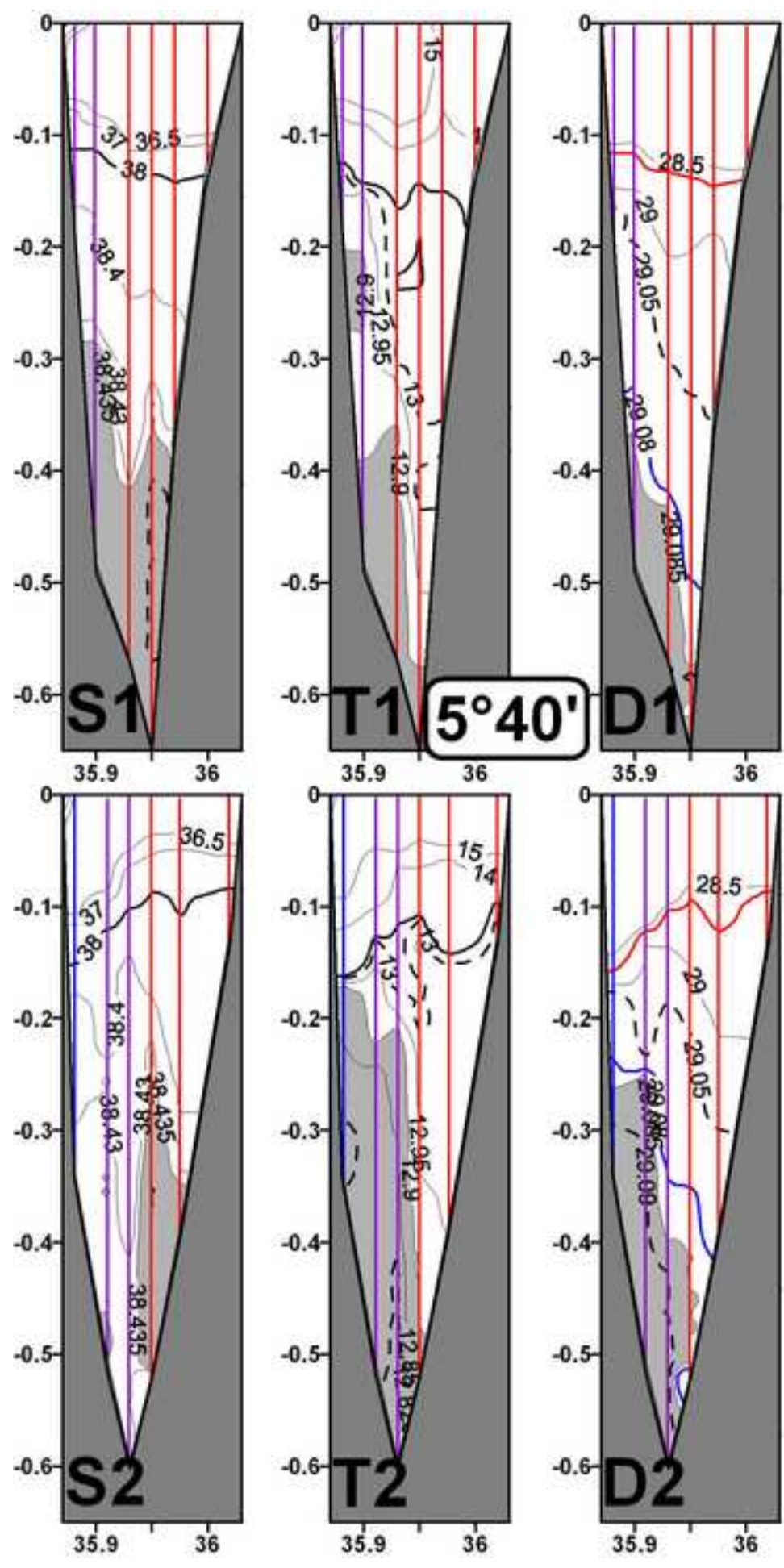


Figure 14  
[Click here to download high resolution image](#)

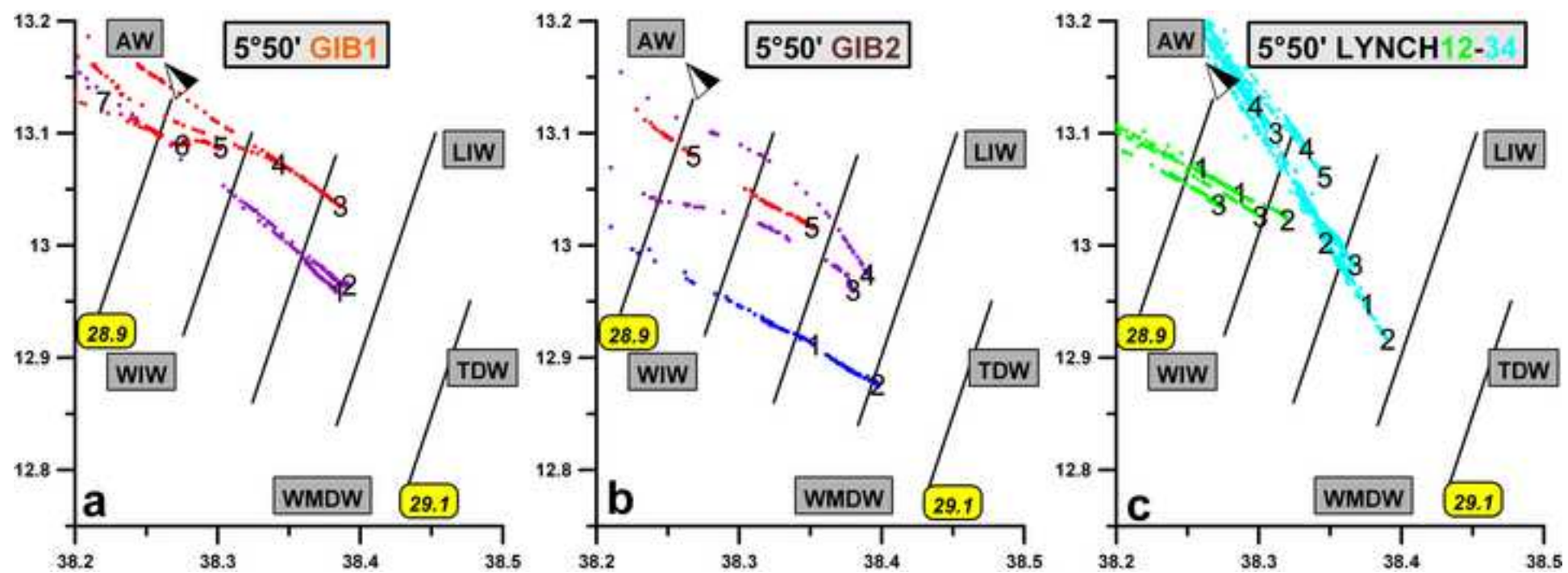


Figure 15  
[Click here to download high resolution image](#)

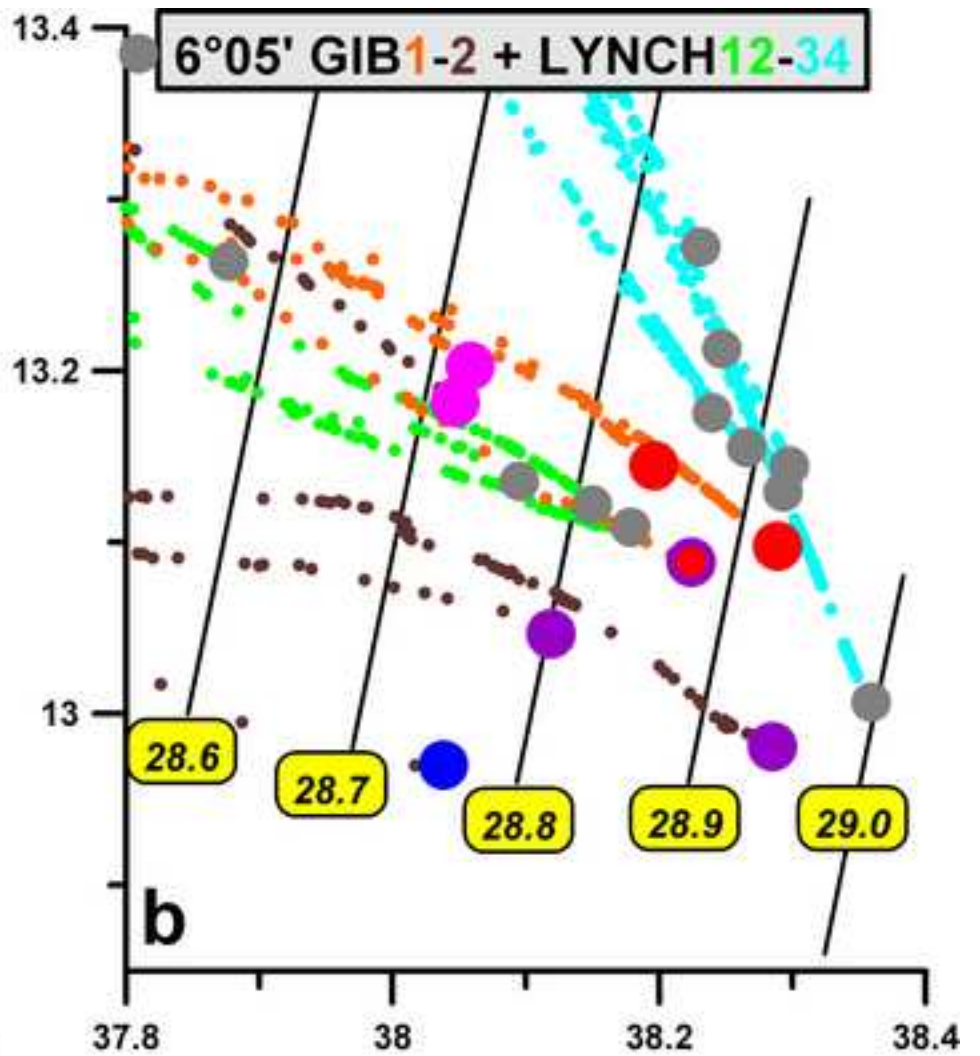
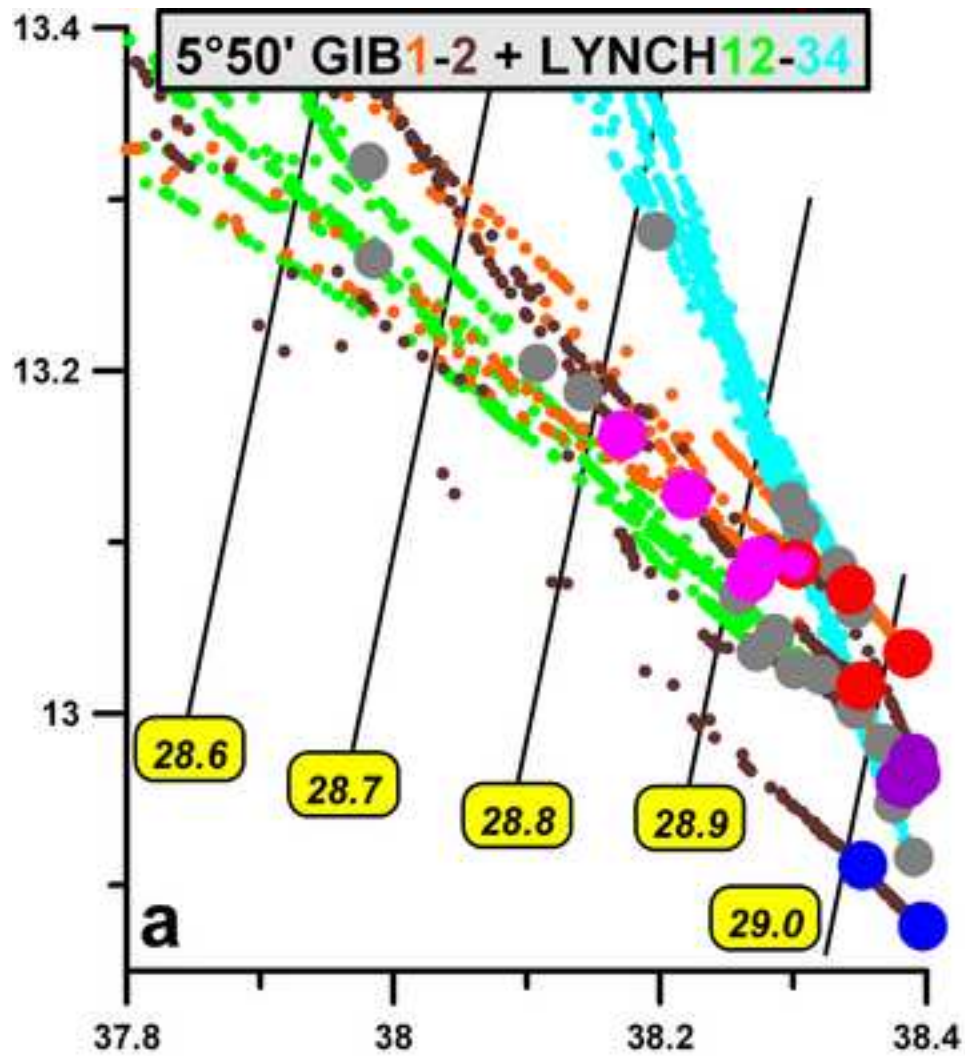




Figure 16B  
[Click here to download high resolution image](#)

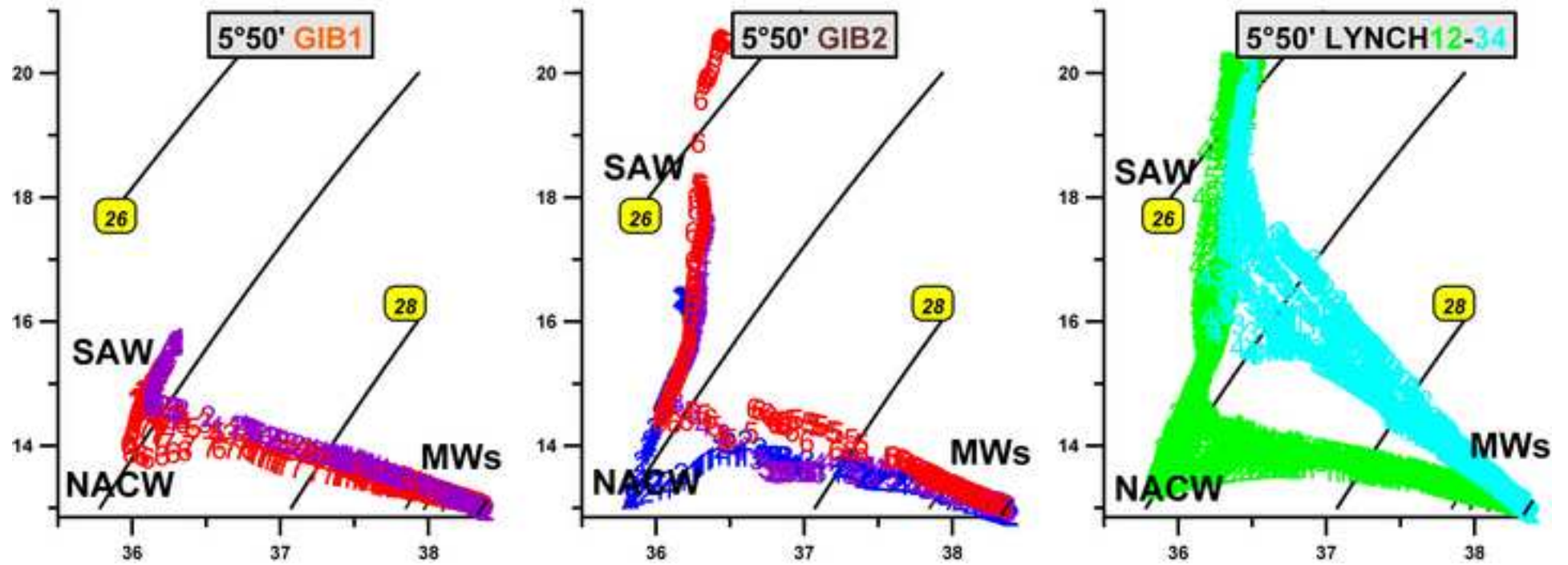


Figure 17  
[Click here to download high resolution image](#)

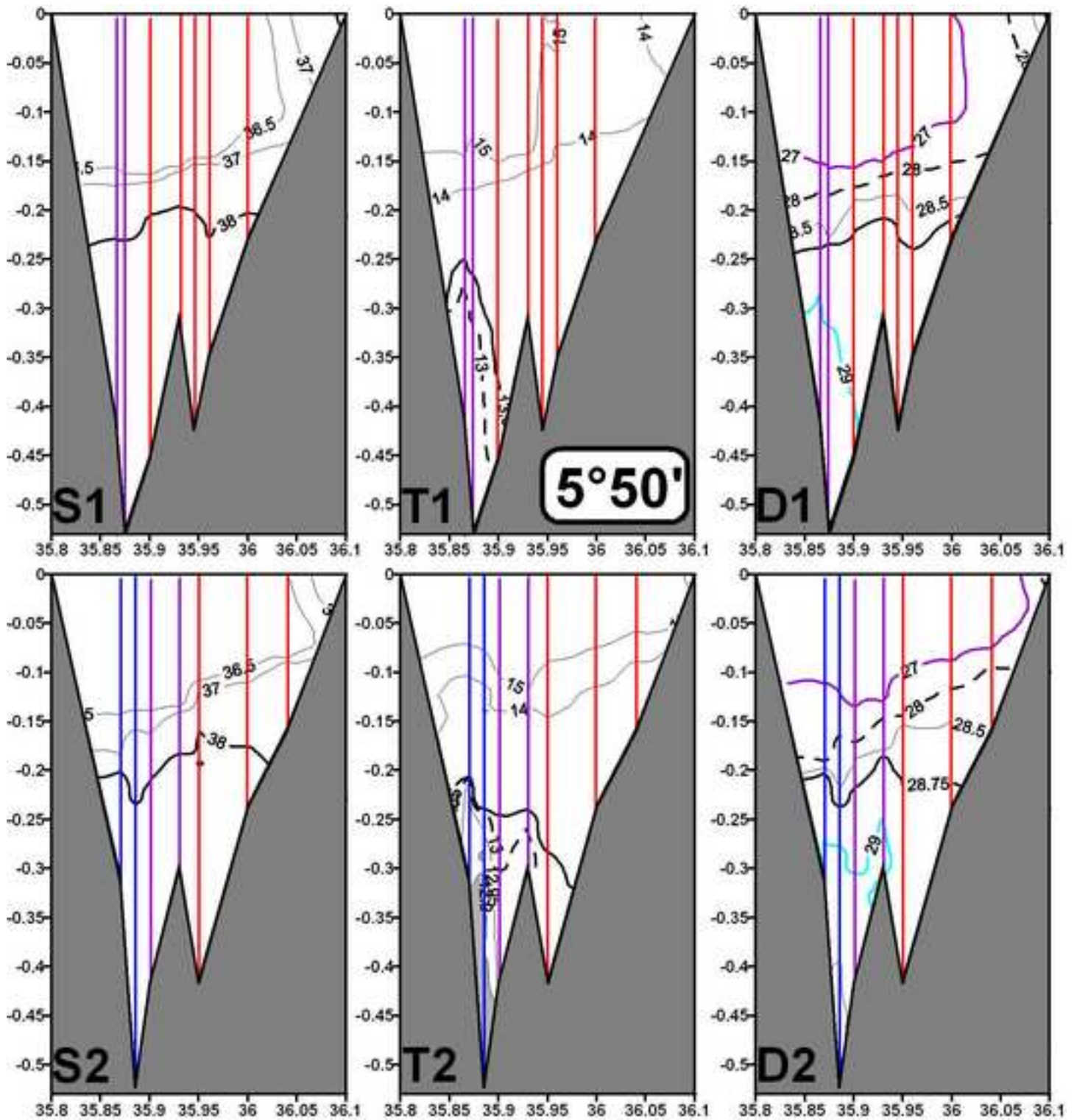




Figure 19  
[Click here to download high resolution image](#)

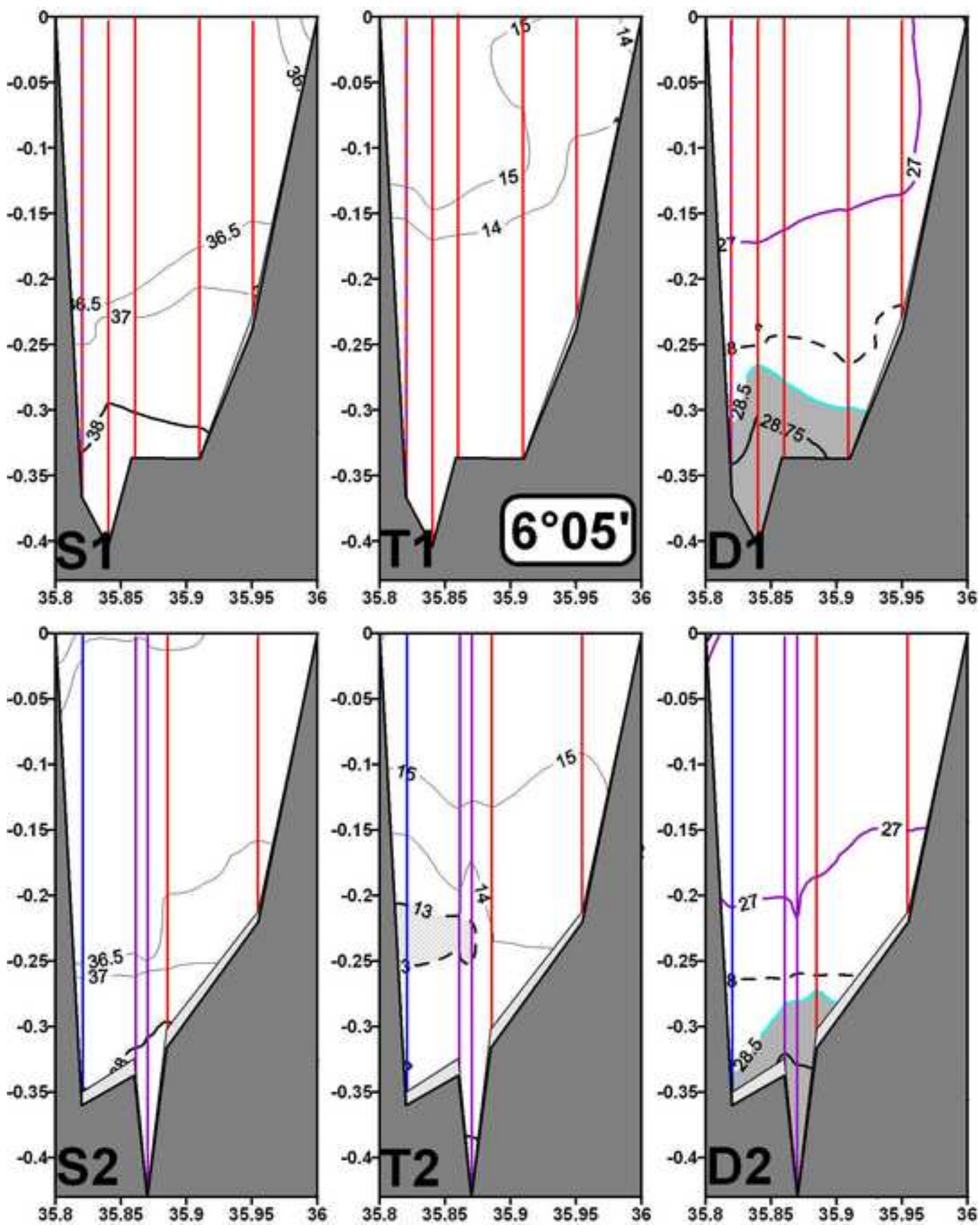


Figure 20  
[Click here to download high resolution image](#)

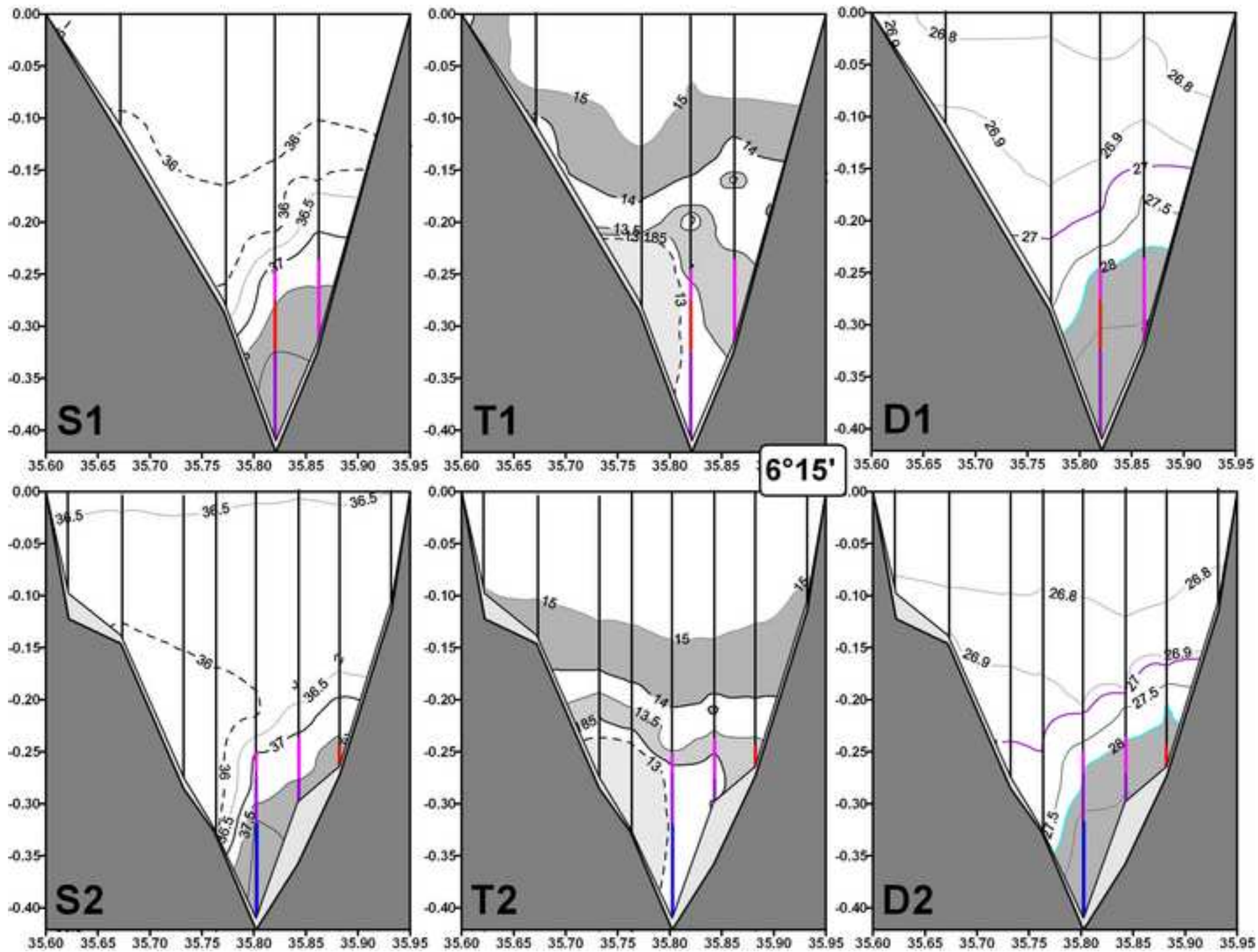


Figure 21  
[Click here to download high resolution image](#)

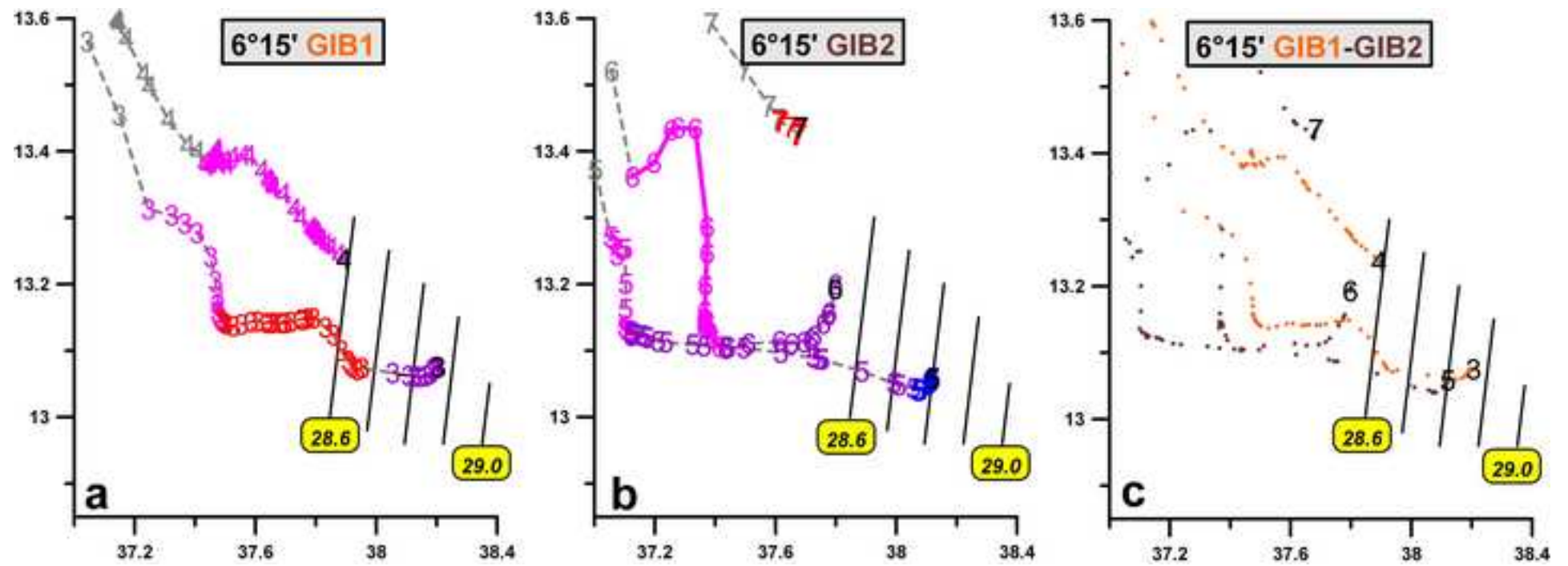


Figure  
[Click here to download high resolution image](#)

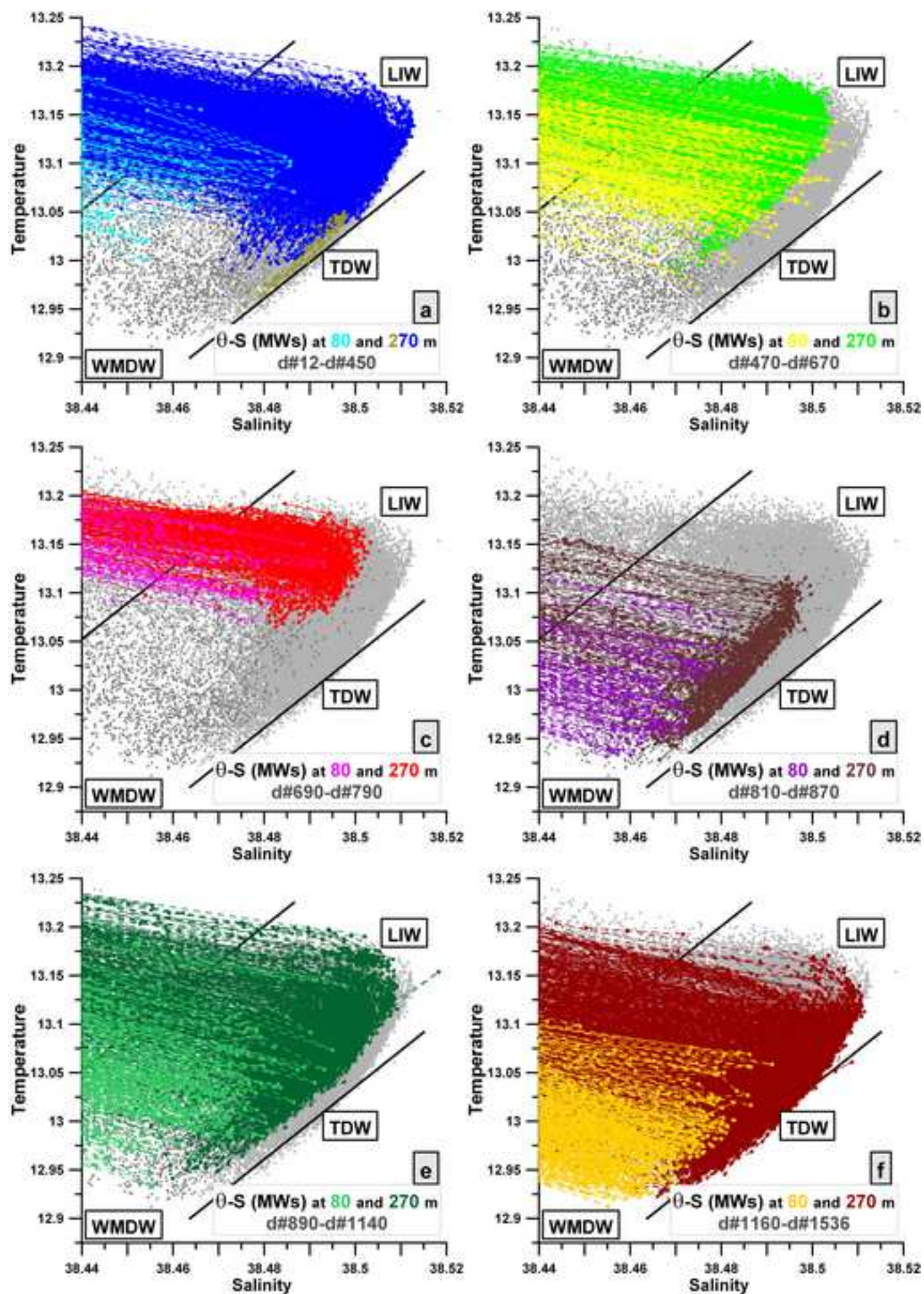


Figure 23  
[Click here to download high resolution image](#)

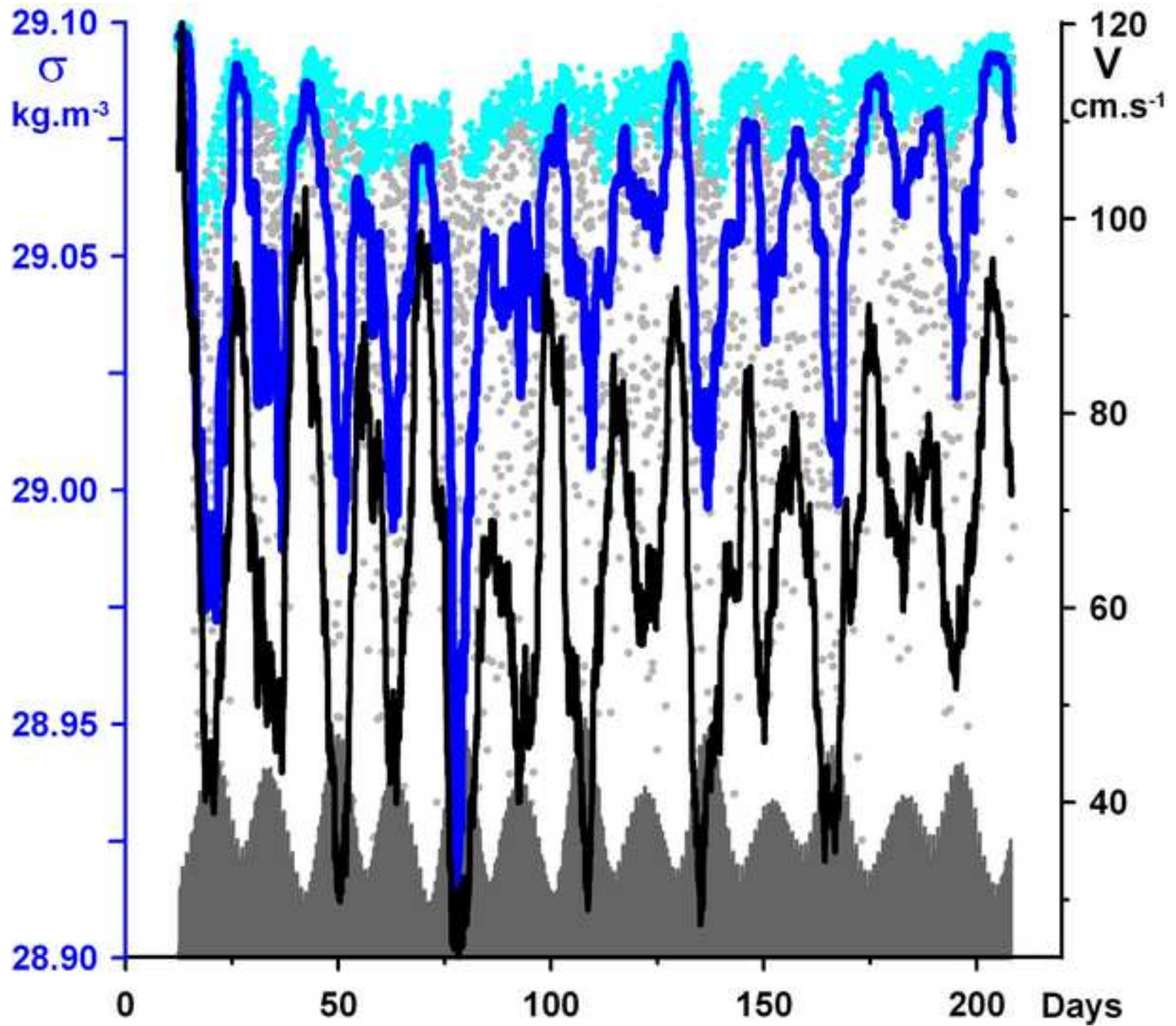


Figure 24  
[Click here to download high resolution image](#)

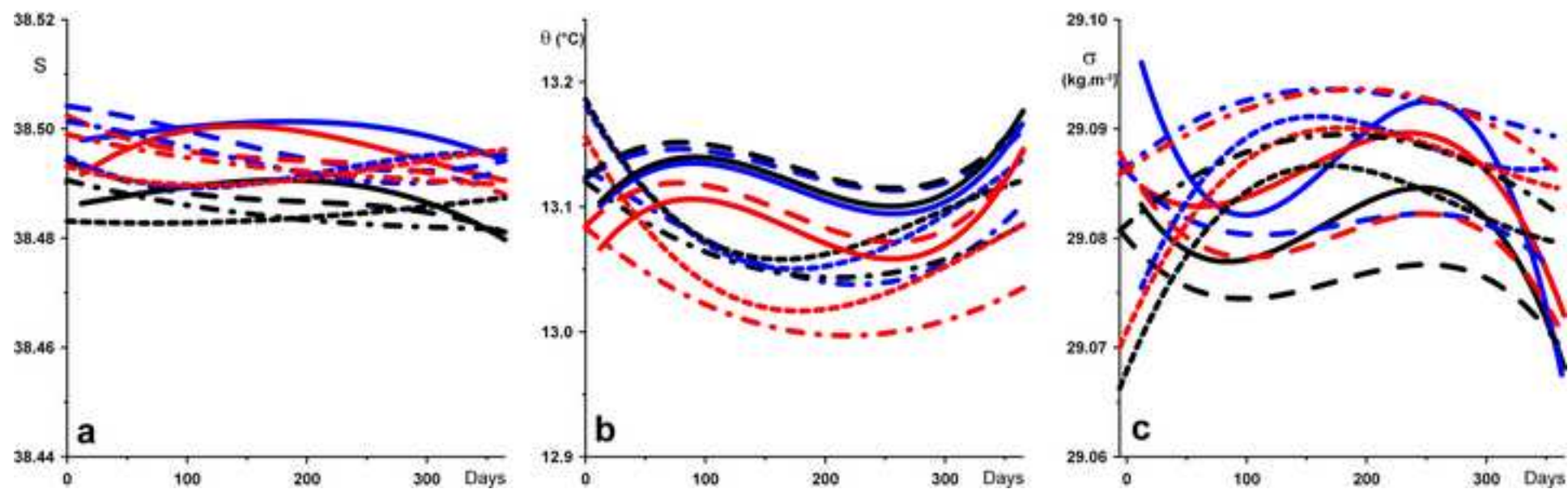


Figure 25

[Click here to download high resolution image](#)

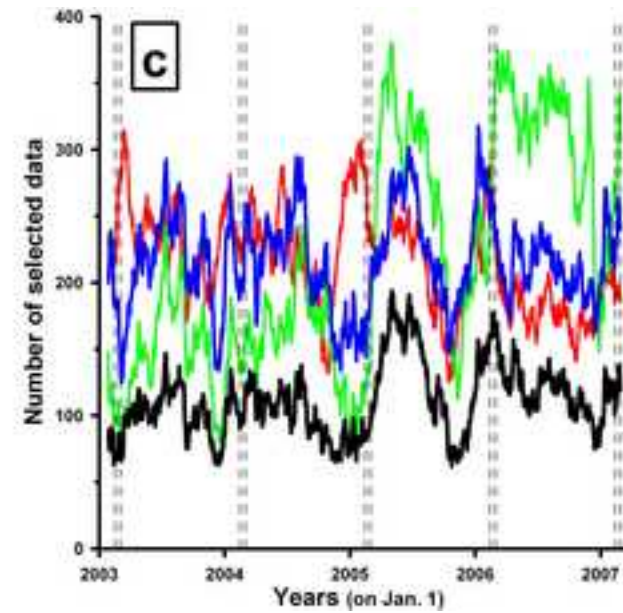
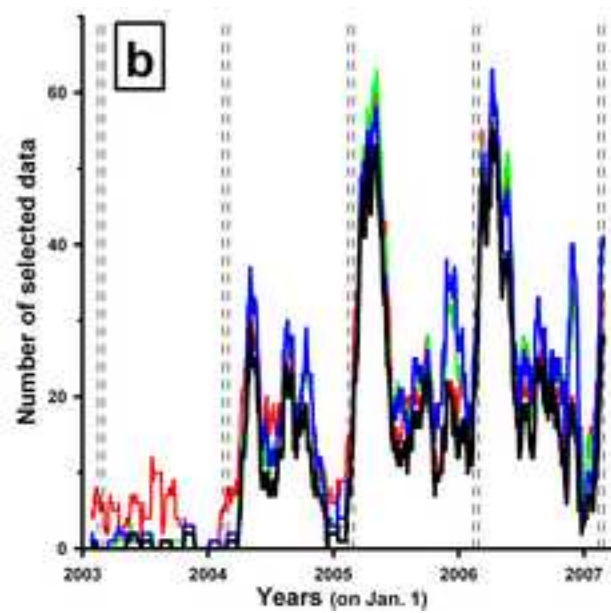
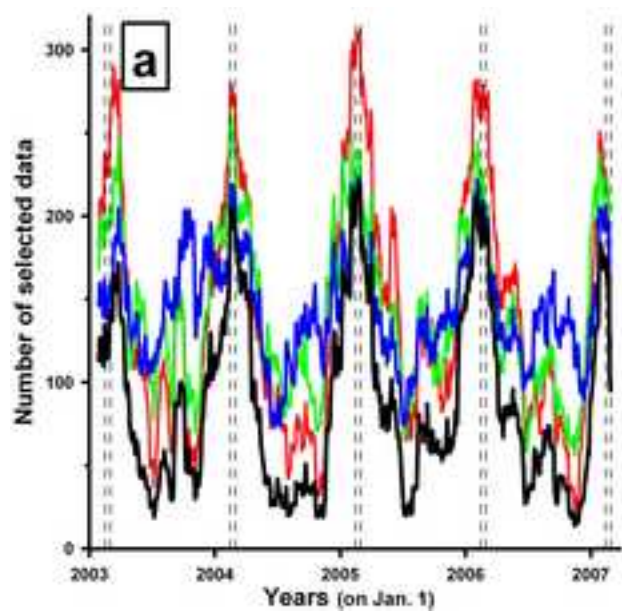


Table 1

GIB1		GIB2	
6°15'	2/04/86 05:19	6°05'	26/09/86 17:21
	06:39,07:49		18:29,19:06,19:42
	2/04/06 09:01		26/09/86 20:22
5°15'	12/04/86 13:32	6°15'	27/09/86 02:37
	14:07,14:52,16:00,17:08,18:29,19:56, 20:53, 12/04/06 21:45		03:57,04:35,05:10,06:00,06:41,07:43
			27/09/86 08:30
5°00'	12/04/86 23:51	5°50'	29/09/86 00:28
	00:36,02:07,03:54,05:40,07:20		01:02,01:42,02:26,03:27,04:13
	13:04:86 08:41		29/09/86 04:44
4°30'	13/04/86 13:44	5°40'	29/09/86 07:32
	15:40,17:10,19:38,22:36,00:57,03:02, 05:05, 14/04/86 05:40		08:09,09:09,09:58,11:07
			29/09/86 12:00
5°30'	16/04/86 17:20	5°30'	29/09/86 15:04
	17:57,19:04,20:12		16:02,17:06,18:00
	16/04/86 22:33		29/09/86 19:20
5°40'	17/04/86 00:16	5°15'	29/09/86 21:57
	00:55,01:33,02:24,03:17		22:47,23:29,01:07,02:16,03:28,04:35, 05:34,06:30, 30/09/86 07:20
	17/04/86 04:07		
5°50'	18/04/86 20:56	5°00'	30/09/86 10:56
	22:02,22:47,23:32,00:25,01:08		12:11,13:35,15:05,16:50,18:21
	19/04/86 02:01		30/09/86 19:27
6°05'	19/04/86 11:52	4°30'	03/10/86 21:21
	12:30,13:00,13:38		22:24,00:17,02:21,05:36,08:00,09:43
	19/04/86 14:17		04/10/86 10:24

Table 2

		$I_{LD} (Z_{min}, \Delta Z, Y)$ m/m/nm ( $10^{-3}$ )	$A_L$ $10^6.m^2$	$A_D$ $10^6.m^2$	$V_L$ $10^{-2}.m.s^{-1}$	$V_D$ $10^{-2}.m.s^{-1}$	$Q_I/Q$ %	$Q_D/Q$ %
4°30'	GIB1	360/60/66.0 (0.5)	35.5	71.0	0.8	0.6	41	59
	GIB2	380/180/66.0 (1.4)	40.0	62.2	1.1	0.4	63	37
5°00'	GIB1	300/120/45.6 (1.4)	22.8	17.9	2.0	1.3	65	35
	GIB2	300/120/45.6 (1.4)	19.8	17.9	2.2	1.5	62	38
5°15'	GIB1	300/200/15.0 (7)	12.9	6.3	4.6	1.8	84	16
	GIB2	320/120/15.0 (4)	11.8	7.0	4.3	2.7	72	28
5°30'	GIB1	360/240/4.8 (27)	5.1	0.8	13	3	97	3
	GIB2	180/320/5.4 (32)	2.7	1.8	21	8	80	20
5°40'	GIB1	320/180/3.0 (32)	3.2	0.4	21	8	95	5
	GIB2	220/160/5.4 (16)	2.3	1.3	22	15	71	29